

1 **Structural complexities and tectonic barriers controlling recent** 2 **seismic activity in the Pollino area (Calabria-Lucania, Southern Italy)** 3 **- constraints from stress inversion and 3D fault model building.**

4
5 Daniele Cirillo^{1-2*}, Cristina Totaro²⁻³, Giusy Lavecchia¹⁻², Barbara Orecchio²⁻³, Rita de Nardis^{1-2*},
6 Debora Presti²⁻³, Federica Ferrarini¹⁻², Simone Bello¹⁻² and Francesco Brozzetti¹⁻²

7
8 ¹ Università degli studi “G. d’Annunzio” Chieti-Pescara, DiSPUTer, via dei Vestini 31, 66100 Chieti, Italy.

9 ² CRUST Centro interUniversitario per l’analisi SismoTettonica tridimensionale, Italy.

10 ³ Università degli studi di Messina, Dipartimento di Scienze Matematiche e Informatiche, Scienze Fisiche e Scienze della
11 Terra, Viale F. Stagno D’Alcontres, 98166, Messina, Italy

12 **Correspondence to:* Daniele Cirillo (daniele.cirillo@unich.it) and Rita de Nardis (rita.denardis@unich.it)

13 **Abstract.** We reconstruct the 3D Fault Model of the structures causative of the 2010-2014 Pollino seismic activity by
14 integrating structural-geological and high-resolution seismological data. We constrained the model at the surface with fault-
15 slip data, and at depth, by using the distributions of selected high-quality relocated hypocenters. Relocations were performed
16 through the non-linear Bayloc algorithm, followed by the double-difference relative location method HypoDD applied to a 3D
17 P-wave velocity model. Geological and seismological data highlight an asymmetric active extensional fault system
18 characterized by an E to NNE-dipping low-angle detachment, with high-angle synthetic splays, and SW- to WSW-dipping,
19 high-angle antithetic faults.

20 Hypocenter clustering and the time-space evolution of the seismicity suggest that two sub-parallel WSW-dipping seismogenic
21 sources, the Rotonda-Campotenese and Morano-Piano di Ruggio faults, are responsible of the 2010-2014 seismicity. The area
22 of the seismogenic patches obtained projecting the hypocenters of the early aftershocks on the 3D fault planes, are consistent
23 with the observed magnitude of the strongest events ($M_w=5.2$, and $M_w=4.3$). Since earthquake-scaling relationships provide
24 maximum expected magnitudes of $M_w=6.4$ for the Rotonda-Campotenese and $M_w=6.2$ for the Morano-Piano di Ruggio faults,
25 we may suppose that, during the sequence, the two structures did not release entirely their seismic potential.

26 The reconstructed 3D fault model also points out the relationships between the activated fault system and the western segment
27 of the Pollino Fault. This latter was not involved in the recent seismic activity but could have acted as a barrier to the southern
28 propagation of the seismogenic faults, limiting their dimensions and the magnitude of the generated earthquakes.

29 1 Introduction

30 In recent years, the reconstruction of 3D Fault Models (hereinafter referred to as 3DFM) obtained by integrating surface and
31 subsurface data, has become an increasingly practiced methodology for seismotectonic studies (*e.g.*, Lavecchia et al., 2017;
32 Castaldo et al., 2018; Klin et al., 2019; Ross et al., 2020; Porreca et al., 2020; Barchi et al., 2021; Di Bucci et al., 2021; SCEC,
33 2021). Detailed structural-geological data are used to define the active faults geometry at the surface whereas high-quality
34 geophysical data are needed to constrain the shape of the sources at depth. The 3DFM building helps determining the spatial
35 relationships and the interactions between adjacent sources and identifying any barriers hampering at depth the propagation of
36 the coseismic rupture. Moreover, such an approach leads to accurately estimating the area of the seismogenic fault, and
37 therefore the expected magnitude.

38

39 In Italy, reconstruction of 3DFM could give important achievements in the Apennine active extensional belt, which is affected
40 by significant seismic activity (ISIDe, 2007; Rovida et al., 2020). This belt consists of ~NW-SE striking Quaternary normal
41 fault systems, and the related basins, located just west or within the culmination zone of the chain (Calamita et al., 1992;
42 Brozzetti and Lavecchia, 1994; Lavecchia et al., 1994, 2021; Barchi et al., 1998; Cinque et al., 2000; Brozzetti, 2011; Ferrarini
43 et al., 2015, 2021). Its structural setting is very complicated due to a polyphase tectonic history characterized by the
44 superposition of Quaternary post-orogenic extension on Miocene-Early Pliocene folds and thrusts and on Jurassic-Cretaceous
45 sin-sedimentary faults (*e.g.*, Elter et al., 1975; Ghisetti and Vezzani, 1982, 1983; Lipmann-Provansal, 1987; Mostardini and
46 Merlini, 1986; Patacca and Scandone, 2007; Vezzani et al., 2010; Ferrarini et al., 2017; Brozzetti et al., 2021).

47

48 Over time, detailed structural geological studies made it possible to recognize several seismogenic faults in the Apennine
49 active extensional belt (Barchi et al., 1999; Galadini and Galli, 2000; Maschio et al., 2005; Brozzetti, 2011) and, in some cases,
50 to document, through paleo-seismological data, their reactivation during the Holocene (Galli et al., 2020). Furthermore, the
51 increasing availability of high-resolution imagery allows fault mapping at the sub-meter scale (*e.g.*, Westoby et al., 2012;
52 Johnson et al., 2014; Cirillo, 2020; Bello et al., 2021b, 2021c), while accurate geophysical prospections (*e.g.*, Ground
53 Penetrating Radar), allows investigating the fault surface at shallow depths (few meters or tens of meters; *e.g.*, Gafarov et al.,
54 2018; Ercoli et al., 2013, 2021). Conversely, the geometries of the faults at depth are rarely available since high-resolution
55 deep geological and geophysical constraints are often lacking (*i.e.*, deep wells and/or seismic profiles). In fact, in the last
56 decades, seismic reflection prospecting and deep-well exploitation for hydrocarbon research, avoided the area affected by
57 active extension, and focused on the eastern front of the chain and on the Adriatic-Bradanic foreland basin system (ViDEPI:
58 www.videpi.com, last access: 19 April 2021).

59 This lack can be compensated with well relocated high-resolution seismological datasets, to be integrated with geological ones.
60 In Italy, datasets of highly precise re-located hypocenters were collected during recent seismic sequences (Chiaraluce et al.,
61 2004, 2005, 2011, 2017; Totaro et al., 2013, 2015). These sequences include thousands of earthquakes (in confined volumes

62 of rock) which appear to roughly connect with the fault traces at the surface. Therefore, such distributions of earthquakes are
 63 generally referred to as ongoing rupture processes affecting an entire, or wide portions of seismogenic faults.
 64 In some cases, very high-resolution hypocenter locations (Chiaraluce et al., 2017; Valoroso et al., 2017), as well as reflection
 65 seismic lines, allow to clearly highlight the seismogenic structures at depth (Sato et al., 1998; Bonini et al., 2014; Lavecchia
 66 et al., 2011, 2012a, 2012b, 2015, 2016; Gracia et al., 2019; Porreca et al., 2018; Barchi et al., 2021).
 67 The study area of this work includes the northern sector of the so-called “Pollino seismic gap” (Fig. 1), in which paleo-
 68 earthquakes up to $M=7$ are documented (Michetti et al., 1997; Cinti et al., 1997, 2002), whereas the location and size of
 69 seismogenic sources are a matter of debate (Michetti et al., 2000; Cinti et al., 2002; Papanikolaou and Roberts, 2007; Brozzetti
 70 et al., 2009, 2017a). Brozzetti et al. (2017a) mapped a set of active faults in the sector between the Mercure, Campotenese, and
 71 Morano Calabro Quaternary basins (Fig. 1a). During 2010-2014, this area was affected by a low to moderate instrumental
 72 seismicity (Pollino seismic activity), climaxing with the 25 October 2012, M_w 5.2 Mormanno earthquake, and characterized
 73 by thousands of recorded events (Totaro et al., 2013, 2015). During the sequence, two others moderate events occurred close
 74 to the village of Morano Calabro: on 28 May 2012 (M_w 4.3) and on 6 June 2014 (M_w 4.0; Fig. 1b). According to Brozzetti et
 75 al. (2017a), the whole seismicity was arranged in two major clusters and a minor one. Each major cluster was associated with
 76 one moderate event and was generated by an independent seismogenic structure. The pre-existence of a seismic network, that
 77 was implemented after the beginning of the sequence, provided a high-quality database of relocated hypocenters (Totaro et al.,
 78 2013, 2015; Brozzetti et al., 2017a).
 79
 80 In such context, we reconstruct the 3DFM involved by the 2010-2014 seismic activity to investigate, at depth, the cross-cut
 81 relationships between the faults having different attitudes and timing of activation. Furthermore, we provide the geometric
 82 parameters of the sources to estimate the expected magnitudes. Finally, we discuss some 3D-seismotectonics methodological
 83 aspects which dwell on the improvements that the proposed procedure provides to the definition of the source model and on
 84 its limits.

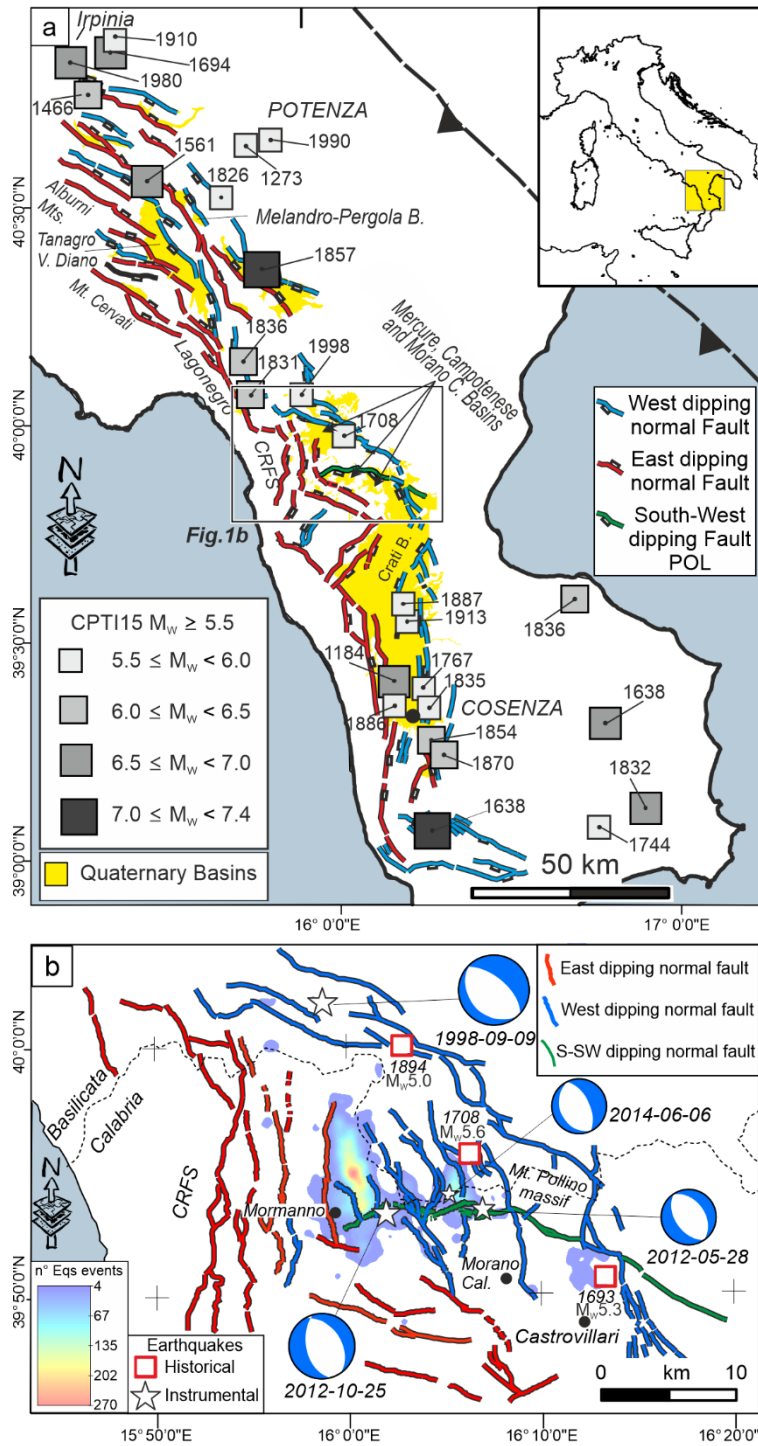


Figure 1: Seismotectonic context of the study area. (a) Active faults of the Southern Apennines with major historical and instrumental earthquakes from Parametric Catalogue of Italian Earthquakes, CPTI15 v3.0 (Rovida et al., 2020, 2021). (b) Normal faults cropping out between the Mercure, Campotenese, Morano Calabro, and Castrovillari Quaternary basins (after

89 Brozzetti et al., 2017a) with distribution of the 2010-2014 Pollino seismic activity (contoured areas) and focal mechanisms of
90 the events with $M_w > 4.0$ (Totaro et al., 2015, 2016).

91

92

93 **2. Geological Setting**

94

95 The Mt. Pollino massif is located at the Calabrian-Lucanian boundary (Fig. 1) in a sector of the Apennines structured during
96 the Middle-Late Miocene contractional tectonics, which affected the western Adria Plate (D'Argenio, 1992; Patacca and
97 Scandone, 2007; Ietto and Barilaro, 1993; Iannace et al. 2004, 2005, 2007). The surface geology in this area is characterized
98 by the superposition of two main tectonic units derived from different paleogeographic domains. These are represented (from
99 bottom to top), by 1) the "Apenninic" units (or "Panormide"; Triassic - Early Miocene), which are characterized by carbonate
100 platform, including the Verbicaro and Pollino Units, locally intruded by basaltic rocks (Ogniben, 1969, 1973; Amodio Morelli
101 et al., 1976; Iannace et al., 2007; Patacca and Scandone, 2007; Vezzani et al., 2010; Tangari et al., 2018), 2) by the "Ligurian"
102 units (Late Jurassic – Early Cretaceous), that consist of ophiolites and deep-sea sedimentary deposits derived from the Western
103 Tethys oceanic basin (Ogniben, 1969, 1973; Amodio Morelli et al., 1976; Liberi et al., 2006; Liberi and Piluso, 2009; Filice
104 et al., 2012, 2013, 2015).

105

106 During uppermost Miocene and Pliocene times, the folds and thrusts pile was displaced by WNW-ESE-striking left-lateral
107 wrench faults (Grandjacquet, 1962; Ghisetti and Vezzani, 1982; Van Dijk et al., 2000). Subsequently, regional-scale
108 extensional fault systems, consisting of E- and W-dipping conjugate normal faults, dissected the Tyrrhenian side and the core
109 of the orogen, which assumed a typical basin and range relief. This Quaternary phase caused the reactivation of the previous
110 strike-slip structures such as the Pollino fault (POL), whose normal to normal-oblique kinematics has been documented since
111 the Early-Middle Pleistocene (Ghisetti and Vezzani, 1982, 1983, Brozzetti et al., 2017a).

112

113 At present, the age of onset of the extensional tectonic is still under discussion; it is referred by some authors to the Early
114 Pleistocene (Ghisetti and Vezzani, 1982; Schiattarella et al., 1994; Papanikolaou and Roberts 2007; Barchi et al., 2007; Mattei
115 et al., 2007; Cifelli et al., 2007; Amicucci et al., 2008; Brozzetti, 2011; Robustelli et al., 2014), while it would not be older
116 than the Middle Pleistocene, according to others (Caiazza et al., 1992; Cinque et al. 1993; Hyppolite et al., 1995; Cello et al.,
117 2003; Giano et al., 2003; Spina et al., 2009; Filice and Seeber, 2019).

118

119 In the Campania-Lucania and north-Calabria sectors of the southern Apennines, the active extensional belt includes three main
120 alignments of normal faults and Quaternary basins, arranged in a right-lateral en-echelon setting (Fig. 1a). From north to south
121 they are: the internal alignment, including the Irpinia fault, the Melandro-Pergola and Agri basins the intermediate one,
122 developing from the Tanagro-Vallo di Diano basins to the Mercure-Campotenese and Morano Calabro basins the external

alignment, developing from the Castrovillari fault to the southern Crati basin (Pantosti and Valensise, 1990, 1993; Ascione et al., 2013; Galli and Peronace, 2014; Ghisetti and Vezzani, 1982, 1983; Barchi et al., 1999, 2007; Blumetti et al., 2002; Amicucci et al., 2008; Maschio et al., 2005; Villani and Pierdominici, 2010; Brozzetti, 2011, Faure Walker et al., 2012; Brozzetti et al., 2009, 2012, 2017a, 2017b; Robustelli et al., 2014; Sgambato et al., 2020; Bello et al., 2021a).

All along the above alignments, the geometry and kinematics of the major normal faults are kinematically compatible with a SW-NE direction of extension (Maschio et al. 2005; Brozzetti, 2011; Brozzetti et al., 2009; 2017a). A similar orientation of the T-Axis is obtained from the focal mechanisms of the major earthquakes from CMT and TDMT databases (Pondrelli et al., 2006; Scognamiglio et al., 2006; Montone and Mariucci., 2016; Totaro et al., 2016) and from GPS data (D'Agostino et al., 2014, Cheloni et al., 2017). The recent activity of these normal fault systems is firstly suggested by the control exerted on the distribution of seismicity, as shown by the location of upper crustal instrumental earthquakes (ISIDE Working Group, 2007; Brozzetti et al., 2009; Totaro et al., 2014, 2015; Cheloni et al., 2017; Napolitano et al., 2020, 2021; Pastori et al., 2021; Sketsiou et al., 2021; De Matteis et al., 2021) and of destructive historical events (Fig. 1; Rovida et al., 2021).

The area affected by the 2010-2014 seismicity extends from the Mercure to the Campotenese and Morano Calabro basins, along the intermediate extensional fault alignment which, according to previous literature, consists of three main sets of genetically-linked normal and normal-oblique active faults (Brozzetti et al., 2017a; Figs 1b, 2; Acronyms list in Supplementary Text 1). The first one, referred to as the Coastal Range Fault Set (CRFS; red lines in Figs 1b, 2) dips E- to NNE and encompasses four sub-parallel major fault segments named, from west to east, Gada-Ciagola (GCG), Papasidero (PPS), Avena (AVN) and Battendiero (BAT). Their strike varies southward from N-S to WNW-ESE.

The other two fault sets strike ~NW-SE and dip ~SW (blue lines in Figs 1b, 2). The western one, developing from Rotonda to Campotenese villages, consists of two main right-stepping en-echelon segments. They are referred to as ROCS system and include the Rotonda-Sambucoso (RSB) and Fosso della Valle-Campotenese (VCT; Fig. 2). The eastern set, including the en-echelon Castello Seluci - Piana Perretti - Timpa della Manca (CSPT), the Viggianello-Piani del Pollino (VPP) and the Castrovillari (CAS) faults, represents the break-away zone of the Quaternary extensional belt. In the area between these two W-dipping sets, the W to NW-dipping Morano Calabro-Piano di Ruggio (MPR) and Gaudolino (GDN) faults show evidence of Late Quaternary activity (Brozzetti et al., 2017a; Fig. 2).

GPS and DInSAR analysis demonstrated as the Pollino area was affected by important deformation rates during the 2010-2014 seismic activity, with increasing and decreasing of slip values due to the temporal and spatial variation of the recorded seismicity (Passarelli et al. 2015).

151

152

153 **3 Seismotectonic Setting**

154

According to Michetti et al. (1997, 2000) and Cinti et al. (1997, 2002), POL and the adjacent CAS faults were associated with at least two strong earthquakes (M 6.5 and M 7.0), occurred in the period 2000-410 B.C. and 500-900 A.D., respectively. The

epicenter of the 8 January 1693 earthquake (M 5.3, CPTI15, Rovida et al., 2020, 2021; Fig. 1b, Fig. 2) is also located within the hanging wall of the CAS and at the footwall of the MPR fault, some kilometers eastward of the 2012 and 2014 Morano Calabro strongest events. The epicenter locations of the M_w 5.5, 1708, and M_w 5.1, 1894 earthquakes (Rovida et al., 2021), close to the northern termination of the RSB and within its hanging wall, allow hypothesizing the latter fault as the possible seismogenic source.

The main instrumental event recorded in the Pollino area is the M_w 5.6 Mercure earthquake (9 September 1998; Fig. 1b), which was followed by some hundred aftershocks and that was associated by Brozzetti et al. (2009) with the SW-dipping CSPT (Fig. 1b, Fig. 2), located some kilometers to the NE of the Mercure basin.

The focal mechanisms of the three strongest earthquakes (M_w 5.2, 25 October 2012-Mormanno; M_w 4.3, 28 May 2012-Morano Calabro; M_w 4.0, 6 June 2014-Morano Calabro) are consistent with extensional (upper crustal) deformations (Montone and Mariucci 2016; Mariucci and Montone 2020).

All the associated WSW-ENE oriented T-axes are also quite parallel to the geological and seismological least compressional axis, as provided by the tensorial analysis in the neighbouring Mercure area (Brozzetti et al., 2009; Ferranti et al., 2017) or derived from borehole breakouts (Montone and Mariucci 2016; Mariucci and Montone 2020), and GPS data (D'Agostino et al., 2014). As discussed by Totaro et al. (2015, 2016) and Brozzetti et al. (2017a), the available focal solutions well correlate with the Quaternary normal faults recognized in the epicentral area, represented by N-S to NNW-SSE-striking (W-dipping) seismogenic sources.

Correlating the hypocenters distribution with the active faults at surface, the seismogenic source of the 25 October 2012 Mormanno Earthquake (M_w 5.2), is identifiable in both the segments of the WSW-dipping ROCS system (RSB and VCT in Fig. 1b, Fig. 2). These faults dip 70° - 75° , at the surface, and would reach a dip of $\sim 55^\circ$ at depth (Brozzetti et al., 2017a). Through similar reasonings, the WSW-dipping MPR fault was suggested to be the causative fault of the eastern Morano Calabro cluster (Fig. 1b) and of its two major events (M_w 4.3, 28 May 2012 and M_w 4.0, 6 June 2014). The fault extends for ~ 7 km in a N170 direction and is co-axial with the W-dipping nodal planes of the two main events of the sequence (Fig. 1b). The partial reactivation of the CAS could be invoked to explain the minor cluster of seismicity recorded at the eastern side of the study area, although some of the events seem to be located at its footwall.

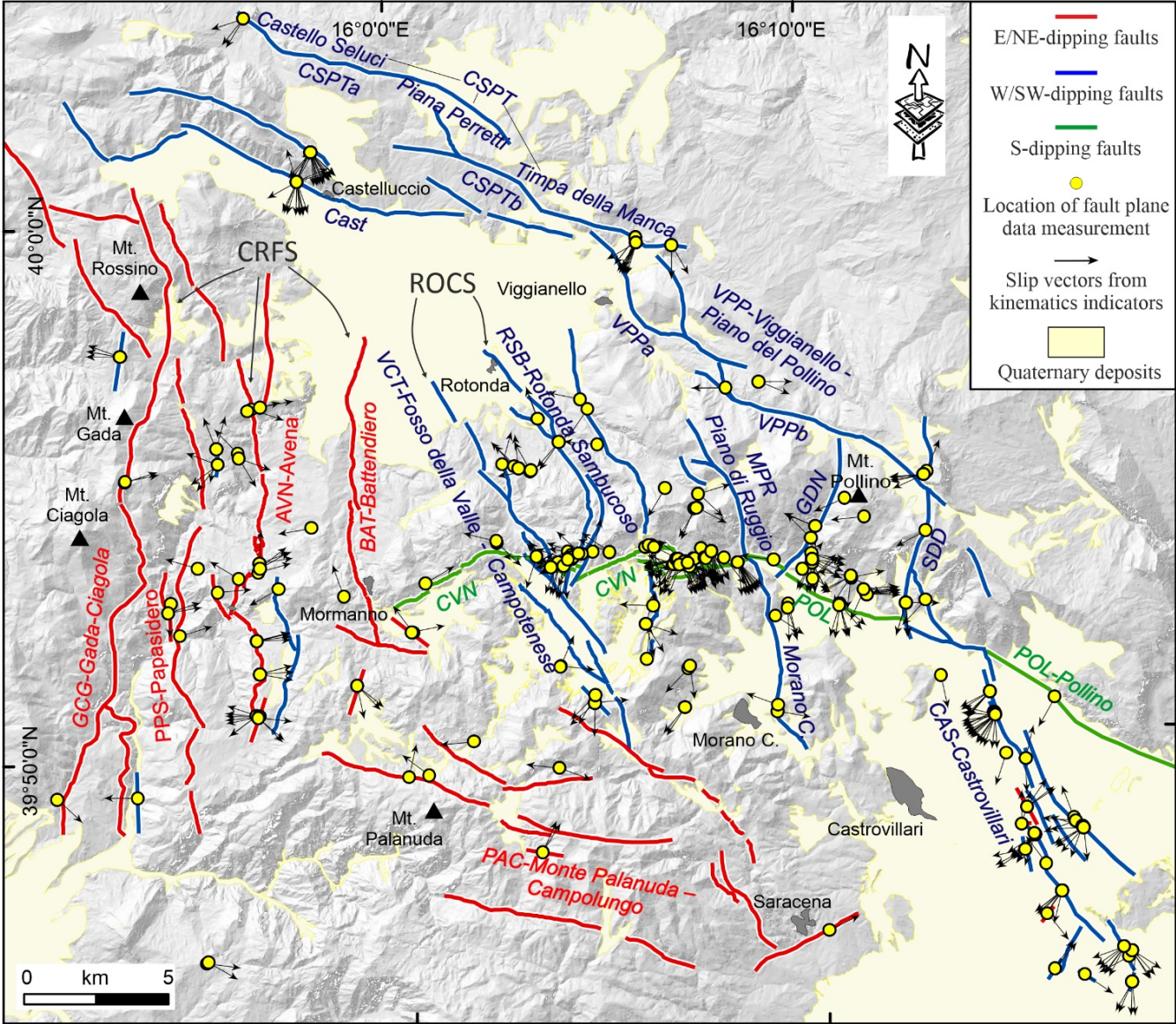
4 Data and Methods

4.1 Structural survey and fault kinematic analysis

We performed a series of fieldwork campaigns, at 1:25.000 scale, in the study area and surrounding sectors, to collect fault-slip data to be integrated with the geological-structural observations reported in Brozzetti et al. (2017a). In addition to traditional survey methods, we used the Fieldmove App (PetEx Ltd., version 2019.1) installed on a tablet computer to acquire the data in the field (e.g., Allmendinger et al., 2017; Novakova and Pavlis, 2017; Testa et al., 2019; Cirillo, 2020), and we

190 managed them in ArcGIS v.10.8 (ArcMap©). Fig. 2 shows the location of the survey sites, considered structurally
 191 homogeneous outcrops falling within a maximum distance of 500 m (see also Supplementary Fig. 2). The overall fault-slip
 192 dataset was first subdivided into minor and local homogenous kinematic subsets, the latter represented as pseudo-focal
 193 mechanisms using FaultKin 8 software (Marrett and Allmendinger, 1990; Allmendinger et al., 2012; Fig 3). The fault/slip data
 194 were subsequently inverted (see following sec. 4.3).

195
 196



197

198 **Figure 2:** Structural Map at the Calabrian-Lucanian boundary (after Brozzetti et al., 2017a) with location of fault-slip data
199 measurements. Fault key: CRFS= Coastal Range Fault Set; GCG= Gada-Ciagola fault; PPS= Papasidero fault; AVN= Avena
200 fault; BAT= Battendiero fault; ROCS= Rotonda-Campotenese fault system; VCT= Fosso della Valle-Campotenese fault;
201 RSB= Rotonda-Sambucoso; CVN= Cozzo Vardo-Cozzo Nisco fault; MPR= Morano Calabro-Piano di Ruggio fault; VPP=
202 Viggianello - Piani del Pollino fault set; VPPa= Viggianello-Prastio fault; VPPb= Vacquarro-Piani del Pollino fault; GDN=
203 Gaudolino fault; POL= Pollino fault; CAS= Castrovillari fault; SDD= Serra Dolcedorme fault; PAC= Monte Palanuda –
204 Campolungo fault; Cast= Castelluccio fault; CSPT= Castello Seluci-Piana Perretti-Timpa della Manca fault; CSPTa= Castello
205 Seluci - Piana Perretti fault; CSPTb= Timpa della Manca - La Fagosa fault.
206
207

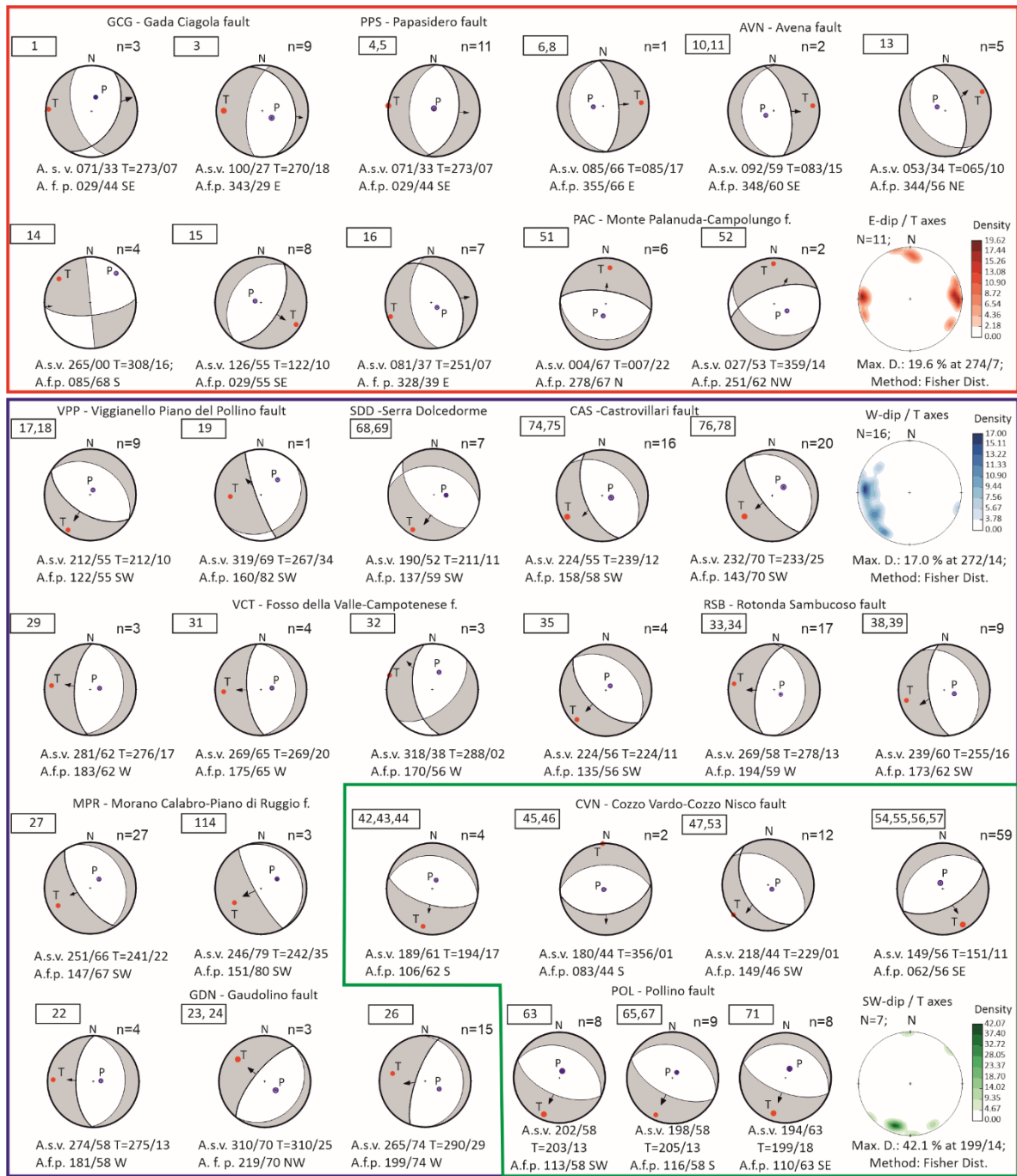


Figure 3: Kinematic analysis and pseudo-focal mechanisms obtained from fault/slip data using the FaultKin 8 software (Allmendinger et al., 2012). Pseudo-focal mechanisms are boxed with different colours on the basis of the fault system to which they belong to (color key as in the map of Fig. 1, Fig. 2). For each fault system, the density contour of the T-axis computed for each focal mechanism is reported (lower hemisphere projection). A.s.v.=Average striae value, A.f.p.=Average

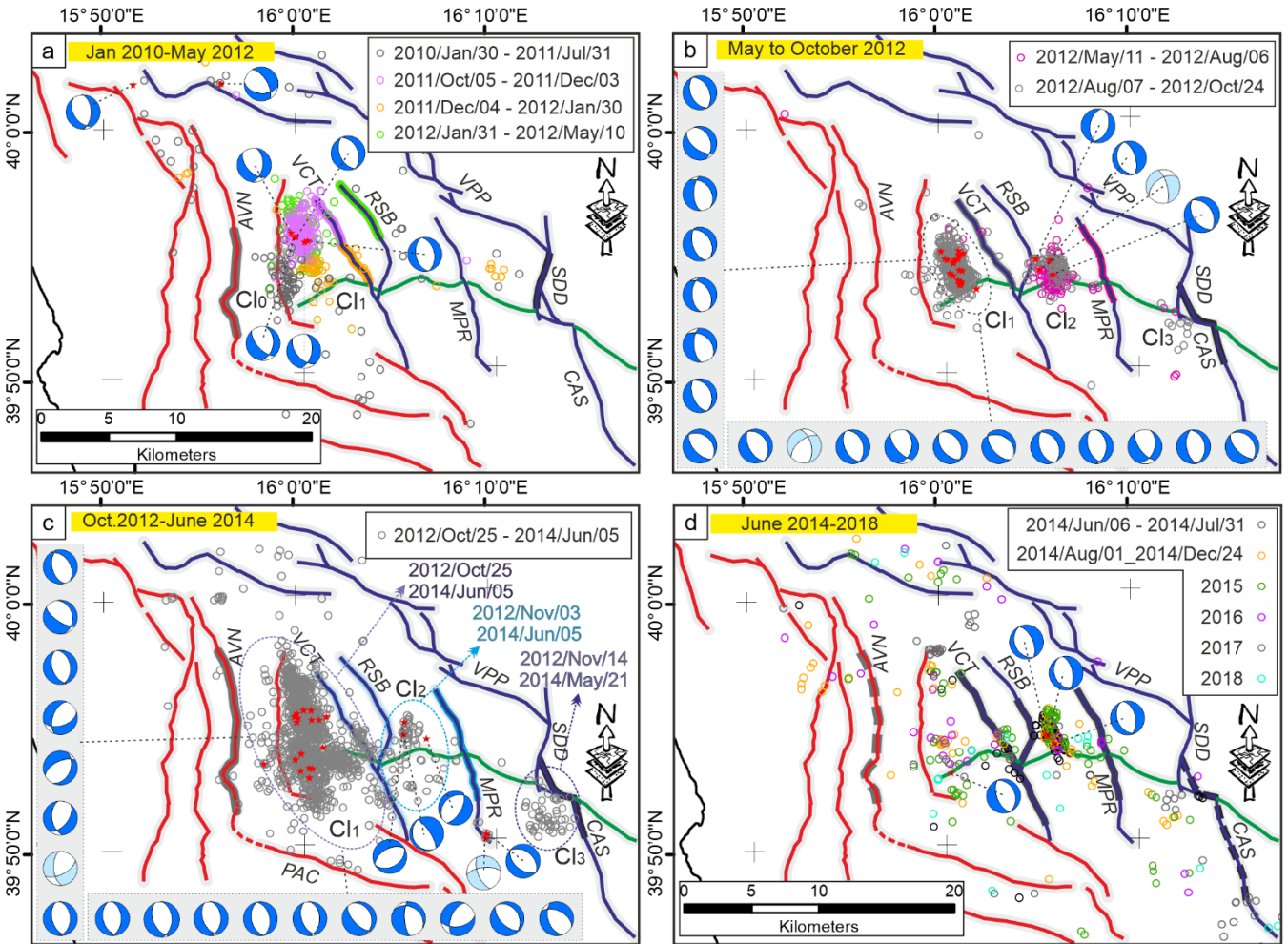
214 fault plane, n =number of fault-plane measurements. Numbers in the rectangles (top left of each focal mechanism) refer to the
215 group of fault/slip data belonging to or neighbouring of a single site (location in Supplementary Fig. 2).

216

217 4.2 Hypocenter location

218

219 To better characterize the 3D features of the tectonic structures located in the study area, we performed a high-quality
220 hypocenter location. We enlarged, with respect to previous works by Totaro et al. (2013, 2015) and Brozzetti et al. (2017a),
221 the time window for earthquake analyses (i.e., January 2010 and October 2018), selecting earthquakes with local magnitude
222 greater than 1.0 and hypocentral depth range 0-30 km from the INGV and the University of Calabria database (www.ingv.it,
223 last access: 19 April 2021; <http://www.sismocal.org>, last access: 19 April 2021). Automatic and manually revised P- and S-
224 wave arrival time picks have been selected for this dataset. The recording network, including both temporary and permanent
225 stations managed by the University of Calabria and INGV (D'Alessandro et al., 2013; Margheriti et al., 2013), consisted of 61
226 stations with a maximum epicentral distance of 150 km (Supplementary Fig. 1). We computed accurate absolute hypocenter
227 locations by applying first the non-linear Bayloc earthquake location algorithm (Presti et al., 2004, 2008) and subsequently the
228 double-difference relative location method HypoDD (v.2; Waldhauser, 2001), and using the 3D velocity model by Orecchio
229 et al. (2011). The Bayloc algorithm gives for each earthquake a probability density cloud with shape and size related to the
230 main factors involved in the location process (e.g., network geometry, picking errors), and allows a generally more accurate
231 estimate of hypocenter parameters and location uncertainties with respect to the more commonly used linearized location
232 methods (e.g., Lomax et al., 2000; Husen and Smith, 2004; Presti et al., 2008). The application of the Bayloc algorithm
233 provides, on average, horizontal and vertical errors of the order of 1.0 and 1.5 km, respectively, allowing us to obtain a well-
234 constrained database. As the second step, we apply the HypoDD algorithm, which minimizes phase delay-time residuals
235 between pairs of events recorded at common stations (Waldhauser and Ellsworth, 2000). We compute the delay times from
236 each event to its 30 nearest neighbours within 10 km distance, and to further ensure the robustness of the double-difference
237 inversion, only event pairs with at least eight phases observed at common stations were used. The final relocated dataset
238 consists of 3109 events (Fig. 4 and Supplementary Fig. 1). During the decade before the 2010-2014 Pollino sequence, the
239 instrumental data available within a range of nearly 75 km from the Mercure basin, referred to background seismic activity
240 (Frepoli et al., 2005; Castello et al., 2006; Brozzetti et al., 2009). A significant seismic activity which affected the region, was
241 the moderate magnitude 1998-1999 Mercure sequence that developed in the northern part of the homonym Quaternary basin
242 (Supplementary Fig. 1; Guerra et al., 2005; Arrigo et al., 2006; Brozzetti et al., 2009) and showed some similarities to the
243 recent Mercure-Pollino sequence (e.g., prevalent kinematics of focal mechanisms and hypocentral depth range). We explored
244 the data available for this seismic activity to compute a high-quality earthquake location, following the procedure described
245 above for the 2010-2018 earthquakes dataset. Since the recording network operating during the 1998-1999 seismic phase was
246 significantly different from today, in terms of the number of stations deployed in the region and their spatial distribution, the
247 available data do not allow to reach the high level of constrain needed to perform the 3D structural model reconstruction.



249

250 **Figure 4:** Time-space evolution of the 2010-2018 seismic activity in the Pollino area. Each panel shows the distribution of
251 focal mechanisms (Totaro et al., 2015, 2016) and epicenters concentrated in a series of neighbouring clusters numbered as Cl
252 0, 1, 2, and 3 from west to east, according to their activation time. See section 5.2 for the sequence description. The Focal
253 mechanisms are classified following Frohlich (2001) kinematics classification (blue beachball= Normal kinematics; light
254 blue= Normal Strike kinematics). Red small circles represent the epicentres of focal mechanism solutions.

255

256 **4.3 Geological and seismological stress tensor inversion**

257

258 To investigate the coherence between the geological and the seismological stress fields, we applied stress tensor inversions to
259 the available fault-slip data (Figs. 2, 3) and focal mechanisms (Fig. 4). We used the ‘TENSOR’ program and the inversion
260 procedure proposed in Delvaux and Sperner (2003). We applied it separately on the different datasets. The procedure computes
261 the orientation of the three principal axes of the stress ellipsoid (σ_1 , σ_2 , σ_3) and the stress ratio $\Phi = (\sigma_2 - \sigma_3) / (\sigma_1 - \sigma_3)$ that

262 optimize the misfit Function (*i.e.*, F5 in ‘TENSOR’ program, described as β in Delvaux and Sperner, 2003). The latter is built
 263 i) to minimize the slip deviation between the observed slip line and resolved shear stress (30° misfit value is not expected to
 264 be exceeded), and ii) to favour higher shear stress magnitudes and lower normal stress to promote slip on the plane. The
 265 inversion procedure provides for the preliminary (kinematic) analysis of data using an improved version of the Right Dihedron
 266 method (Angelier and Mechler, 1977) to determine the starting model parameters (*e.g.*, the reduced stress tensor). The stress
 267 ellipsoid is then computed through a 4D grid-search inversion involving several runs during which the reduced tensor is rotated
 268 around each stress axis with a decreasing range of variability (from $\pm 45^\circ$ to $\pm 5^\circ$), and the full range of Φ values (0-1) is
 269 checked. Each step attempts to find the parameters that minimize the misfit function and that are used as a starting point for
 270 the next run (see for details Delvaux and Sperner, 2003).
 271 The geological data input consists of 268 quality selected fault/slip data measured in the study area (Fig. 2, 3). During the
 272 formal inversion, the same weight value was assigned to each fault. The seismological data input is represented (initially) by
 273 both nodal planes of each focal mechanism; afterwards, the plane that is best explained by the stress tensor in terms of the
 274 smallest misfit function is considered as the actual fault plane (Delvaux and Barth, 2010). The inverted seismological data are
 275 represented by focal mechanisms from Totaro et al. (2015, 2016) and reported in Fig. 4. An exponential weighting factor
 276 (corresponding to the earthquake magnitudes) has been assigned to account for the prevailing kinematics of the most energetic
 277 events. The final inversion (Fig. 5) includes only the fault- and focal-planes that are best fitted by a uniform stress field (Gephart
 278 and Forsyth, 1984).
 279

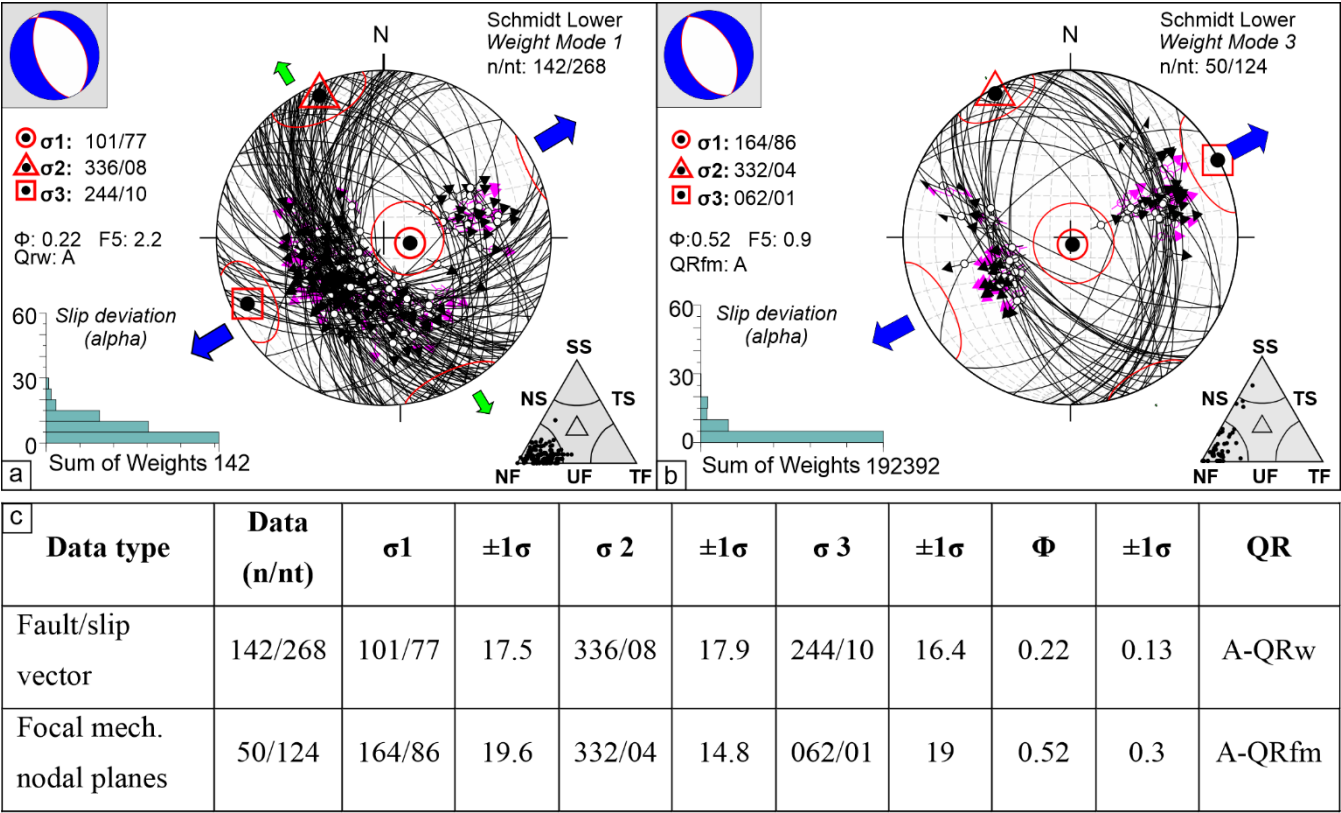


Figure 5: Stress inversion results for the geological- (a) and seismological (b) data. On the lower hemisphere Schmidt nets, the pairs fault plane/slickensline pairs (a) and focal plane/kinematic indicators (rake) (b) are reported (great circles represent the fault planes; the dark and pink arrows indicate the measured slip directions (or rake) and resolved shear stress respectively). The histograms represent the corresponding misfit angles vs the number of data points; nt = total number of fault data; n = number of successfully inverted fault data; σ_1 , σ_2 , σ_3 = principal stress axes; Φ = stress ratio = $(\sigma_2 - \sigma_3) / (\sigma_1 - \sigma_3)$; the quality ranking factors (QR) and the stress inversion parameters with associated uncertainties (1σ standard deviations) are listed in panel (c). On the small upper left nets, the computed stress field represented as a focal mechanism is also reported. The triangles reported on the lower right corner of each panel (a) and (b) show the kinematic classification of data according to Frohlich (2001). (c) Geological and seismological stress tensor parameters computed starting from slip-vector measurements collected along the investigated fault systems (Figs. 2, 3) and focal mechanisms, respectively (see. Sect. 3 and Fig. 4). Key: nt = total number of data (e.g., plane/slickensline); n = inverted data; σ_1 , σ_2 , σ_3 = principal stress axes; Φ = stress ratio = $(\sigma_2 - \sigma_3) / (\sigma_1 - \sigma_3)$. QR = quality ranking: AQRw as in Sperner et al. (2003) and A-QRfm as in Heidbach et al. (2010).

4.4 3D Model building

Following the methodology defined by the Community Fault Model of Southern California (Nicholson et al., 2014; Nicholson

299 et al., 2015; Plesch et al., 2014), also applied for recent Italian earthquakes (Lavecchia et al., 2017; Castaldo et al., 2018; Bello
300 et al., 2021a), we obtained the 3DFM of the Pollino area by integrating Quaternary fault mapping (Brozzetti et al., 2009,
301 2017a; this paper) with high-quality seismicity dataset (2010-2018), and by using the Move suite software v. 2019.1 (Petroleum
302 Experts Ltd).

303

304 In particular, we created several sets of closely spaced transects (distance=2 km) to cross and sample the seismogenic fault
305 zones in different directions (Fig. 6). The first two sets (oriented SW-NE and NW-SE) are respectively ~perpendicular (e.g.,
306 sections a, b in Fig. 6) and ~sub-parallel (e.g., sections c-e in Fig. 6) to the ROCS (VCT and RSB), and MPR active faults
307 (e.g., sections f in Fig. 6). A further NNE-SSW-striking set of transects was traced ~ perpendicular to the active fault
308 alignment bounding eastward the study area, which includes the CSPT and VPP faults (sections g and h in Fig. 6).

309 The 3DFM building was carried out following three steps graphically depicted in Fig. 7 and synthetically described below.

310

311 *Step 1 - Extrusion of fault traces to shallow depth*

312 The traces of the Quaternary faults are “extruded” to a pre-set depth of 2 km b.s.l, according to the fault planes dip
313 measured in the field. In the absence of measured dip-angles, we assumed a fixed value of 60° . The obtained so-called
314 “fault ribbons” are rimmed upward by the topographic surface (a 10 m-resolution DEM; Tarquini et al., 2012).

315

316 *Step 2 - Down-dip extrapolation of the faults along seismological sections*

317 Starting from the analysis of the seismological transects (Fig. 6), we traced the deep geometries by connecting the fault
318 ribbons with the seismicity clusters at depth (Fig. 7b,c) downward to the base of the seismogenic layer.

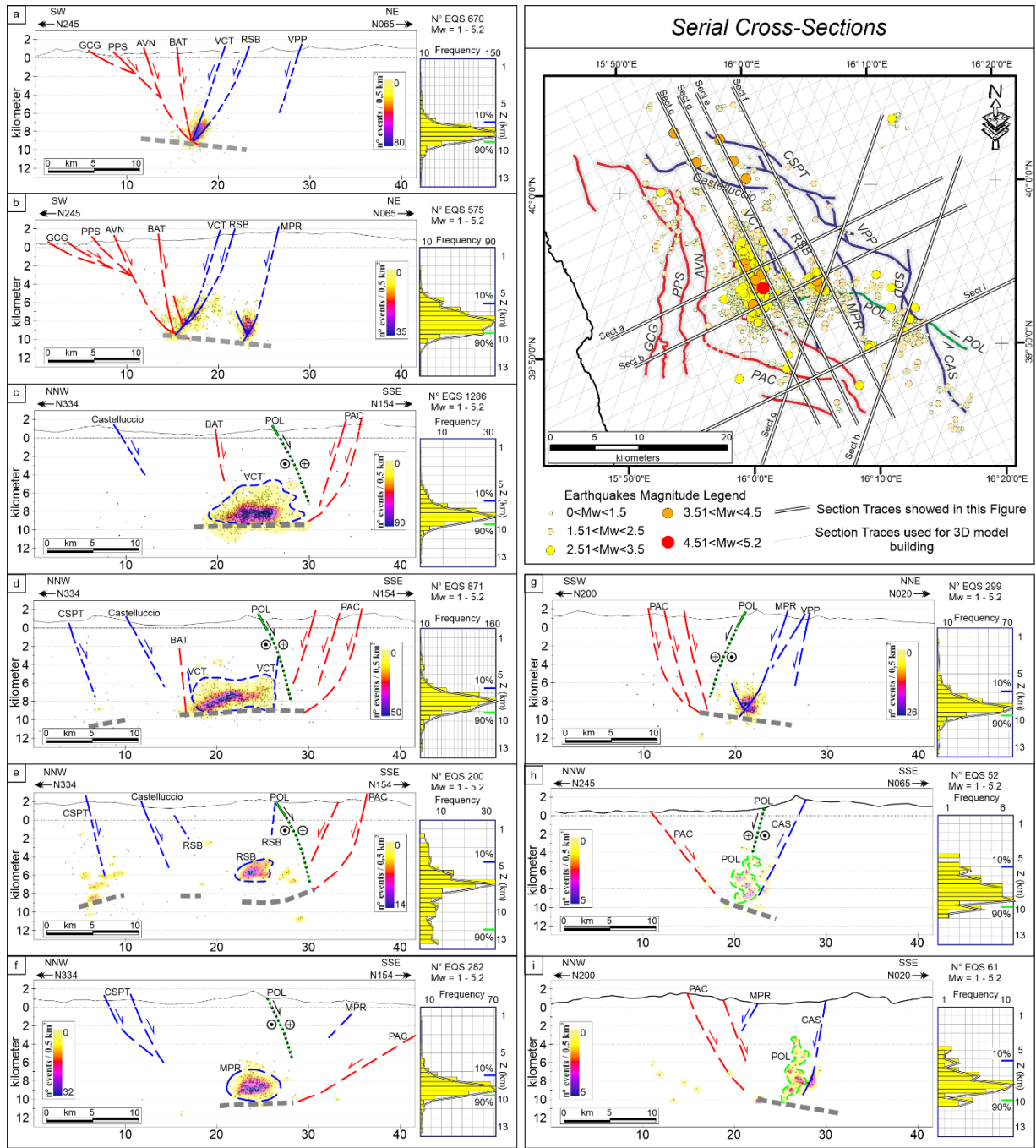
319

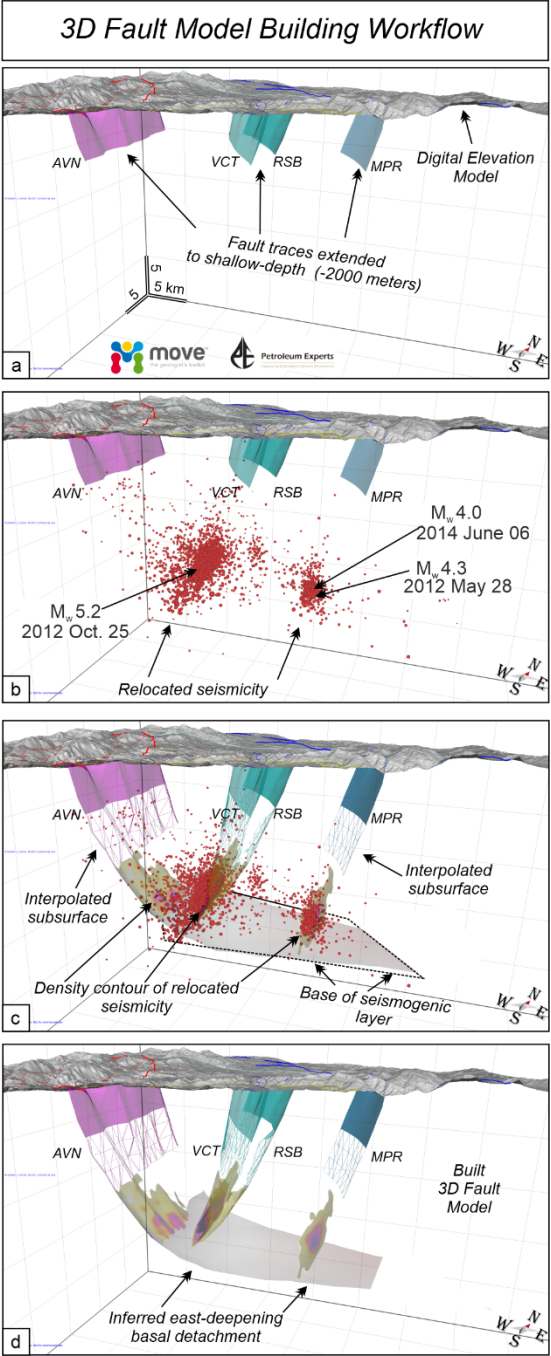
320 *Step3 - Building of 3D fault surfaces*

321 This step allows reaching the final 3D reconstruction (Fig. 7c,d) by interpolating, through the Delaunay triangulation
322 method (Delaunay, 1934), all the fault lines as interpreted along the seismological cross-sections (Step 2). The result is
323 the fault plane surface that best approximates and connects the clusters of seismicity and the surface geology (represented
324 by the fault traces extruded).

325

326





334

335

336

337

338

Figure 7: 3D fault model building, from the surface (10 m-resolution DEM from Tarquini et al., 2012) to the base of the seismogenic layer. Faults acronyms as in Fig. 2. (a) “Fault ribbons” obtained by extruding the fault traces mapped at the surface down to 2 km depth and considering the fault dip-angles measured in the field. (b) 3D fault model as in (a) with the relocated seismicity. (c) Fault extrapolation at (seismogenic) depth through the clusters of hypocenters; the modelled faults connect the

339 ribbons with the zones at the depth where concentrations of hypocenters are higher. The density contours of the seismicity and
340 the base of the seismogenic layer are also shown (see also panel d). (d) Final 3D fault model obtained integrating the detailed
341 Quaternary fault pattern with the high-quality 2010-2018 seismicity dataset.
342

343 **5 Results**

344 **5.1 Geological and Seismological Stress Tensors**

345
346 The computed geological stress tensor (Fig. 5) shows a relevant percentage of fault/slip vector pairs (~53%) consistent with a
347 uniform extensional stress field which is characterized by a N244 trending- and sub-horizontal σ_3 . The stress ratio
348 $\Phi=0.22\pm0.13$ and the rank quality is QRw=A (ranking as in Sperner et al., 2003). Nearly all the kinematic axes related to the
349 inverted data belong to a normal-fault regime, as also pointed out by the triangle in Fig. 5 (Frohlich 2001).
350 The seismological stress tensor (Fig. 5b) obtained from inverting 50 actual fault planes (nt = 124 nodal planes) shows a normal
351 fault regime with an ENE-WSW trending and sub-horizontal σ_3 (N062/01 ± 19). The stress ratio $\Phi=0.52 \pm 0.3$ and the rank
352 quality is QRfm=A (ranking as in Heidbach et al., 2010). Most of the nodal planes show normal-fault kinematics (see Fig. 5b).
353 In both the inversions, a normal-fault regime with sub-horizontal and collinear (~SW-NE trending) σ_3 -axis has been obtained.
354 This result points out the coherence between the geological (long-term) and the present-day stress field and the persistence of
355 this extensional regime at least since the Middle Pleistocene (Brozzetti et al., 2017a).
356 In addition, it is worth noticing as 76% of the successfully inverted fault/slip vector pairs are related to the active fault planes
357 belonging to the E- and W-dipping domains (Fig. 5a), while the remaining 24% include data related to the S-dipping system
358 (CVN and POL). The evidence together with the similarity between the computed stress tensors, is consistent with the prevalent
359 activation, in the Late Quaternary, of the E- and W-dipping fault systems
360
361

362 **5.2 Time-space evolution of the Pollino sequence**

363
364 The 2010-2018 seismic activity in the Pollino-Mercure area followed a peculiar evolution over time (Fig. 4) with epicenters
365 concentrated in a series of neighbouring clusters, numbered as Cluster 0, 1, 2, and 3, from west to east, according to their
366 activation time. Such clusters, independent and unconnected to each other, are related to fault segments that are not in an along-
367 strike continuity.
368

369 Cluster 0 (30/01/2010 - 31/07/2011) includes low magnitude ($1.0 \leq M_L \leq 2.9$) activity located in an NNE-SSW oriented sector
370 at the western boundary of the epicentral area. It is delimited westward by the more external segment of the E-dipping CRFS.
371 Cluster 1 started after 05/10/2011 and lasted for the entire 2011-2014 seismic activity. It extended continuously, both
372 northward and southward, reaching a NW-SE length of ~12 km (Fig. 4a-c). It comprehends the higher number of earthquakes

373 and is largely the major cluster as regards the wideness ($\sim 60 \text{ km}^2$) and energy release. It includes 30 events with $M_L \geq 3.0$
374 besides the 25 October 2012 strongest event of the whole Pollino seismic activity. During the 2015-2018 interval, Cluster 1
375 area was affected by low seismic activity, mostly distributed in its northern and southern portions; conversely, its central part,
376 where epicenters were particularly dense between 2011 and 2014, became less active. Overall, the surface extent of Cluster 1,
377 which partly overlaps with Cluster 0, is limited eastward by the W-dipping RSB and VCT faults. Its southern boundary nearly
378 coincides with the southeastern continuation of the AVN fault (PAC, Fig. 4c).

379 Cluster 2 started in May 2012 in the sector between the two WSW-dipping RSB and the MPR faults. It elongates in N-S
380 direction, for $\sim 7 \text{ km}$ to the northwest of the Morano Calabro town. Afterward, it was nearly continuously active, particularly
381 during the periods May 2012 - October 2014 (Fig. 4b,c); also in the period 2015-2018, significant seismicity persisted (Fig.
382 4d). Cluster 2 includes mainly low-magnitude events besides the strongest ones of 28 May 2012 and 6 June 2014 and three
383 other earthquakes with $3.0 \leq M_L \leq 3.5$.

384 Further east, in the sector comprised between MPR and the alignment VPP-SDD-CAS faults, a minor cluster of seismicity
385 (Cluster 3) develop since December 2011 (Fig. 4a). Since then (2011-2018), it was affected by poor and low-magnitude
386 seismicity, which, however, was clearly above the threshold of background seismicity, with two $M_L=3.0$ events (Fig. 4a-d).

387

388

389 **5.3 3D Fault Model of the Pollino area fault system**

390

391 The obtained 3DFM (Fig. 8), which includes the seismogenic fault system involved during and after the 2010-2014 Pollino
392 seismic activity (CRFS, ROCS, and MPR), also encompasses those faults (GCG, PPS, AVN, BAT, CSPT, VPP, SDD, CAS)
393 that, while showing no direct evidence of recent seismic activity, play a significant role in the seismotectonic frame of the
394 area.

395 The westernmost fault structures (*i.e.*, GCG and PPS), whose deep geometry is not strictly constrained by subsurface data,
396 have been interpreted according to the structural extensional style proposed by Brozzetti et al. (2017a). The latter is coherent
397 with the reconstructions of the active extensional belt of the southern and central Apennines described in the literature (Barchi
398 et al., 2007; Amicucci et al., 2008; Brozzetti et al., 2011, 2017a, 2017b; Lavecchia et al., 2017). Overall, this style is
399 characterized by an asymmetric extension driven by a low-angle (20° to 35°) E-dipping detachment fault, which represents
400 the basal decollement of all the other extensional structures. In the model, all the faults are traced at the surface with their dip-
401 angle as measured in outcrop and evolve downward with nearly-listric geometries to join the detachment at increasing depth
402 from west to east. The latter represents the structurally controlled base of the seismogenic layer. The GCG (Figs 1b, 8), which
403 crops out at low-angle and overcomes all the other east-dipping faults (in terms of both slip and associate extension), is the
404 currently inactive break-away zone of such a detachment. The AVN and BAT (Figs 2, 8), which are the easternmost E-dipping
405 splays, are suggested to be active and seismogenic, being possibly the causative structures of the Cluster 0 of hypocenters
406 (Fig. 4a). Cluster 1 and Cluster 2, which are downward confined by the E-dipping detachment, confirm the activity of the W-

407 SW-dipping ROCS and MPR faults, that we consider them the main geological structures involved during the 2010-2014
408 seismic activity (Figs. 4 and 8a,a1). Further east, the 3DFM has been widened to include the W-dipping CSPT and VPP faults,
409 considered the outer seismogenic front of the extensional system. The along-strike continuity of POL and CVN is interrupted
410 by the W-dipping ROCS and MPR faults (Fig. 8c,d), coherently with the cross-cut relationships observed in the field (Fig. 2).
411 The deep geometry of POL and CVN is interrupted by the NNE-dipping AVN (Fig. 8d), which acts as the southern and basal
412 boundary of the entire active fault system.

413 Finally, the 3DFM shows that almost the whole 2010-2018 seismicity correlate with the W-dipping structures but without
414 affecting their southern termination zones. In other words, no or very few events locate south of the intersection with POL
415 and CVN faults. This latter observation suggests that although the POL and CVN did not play an active role in causing the
416 considered seismicity, they play a significant role in influencing its distribution.

417

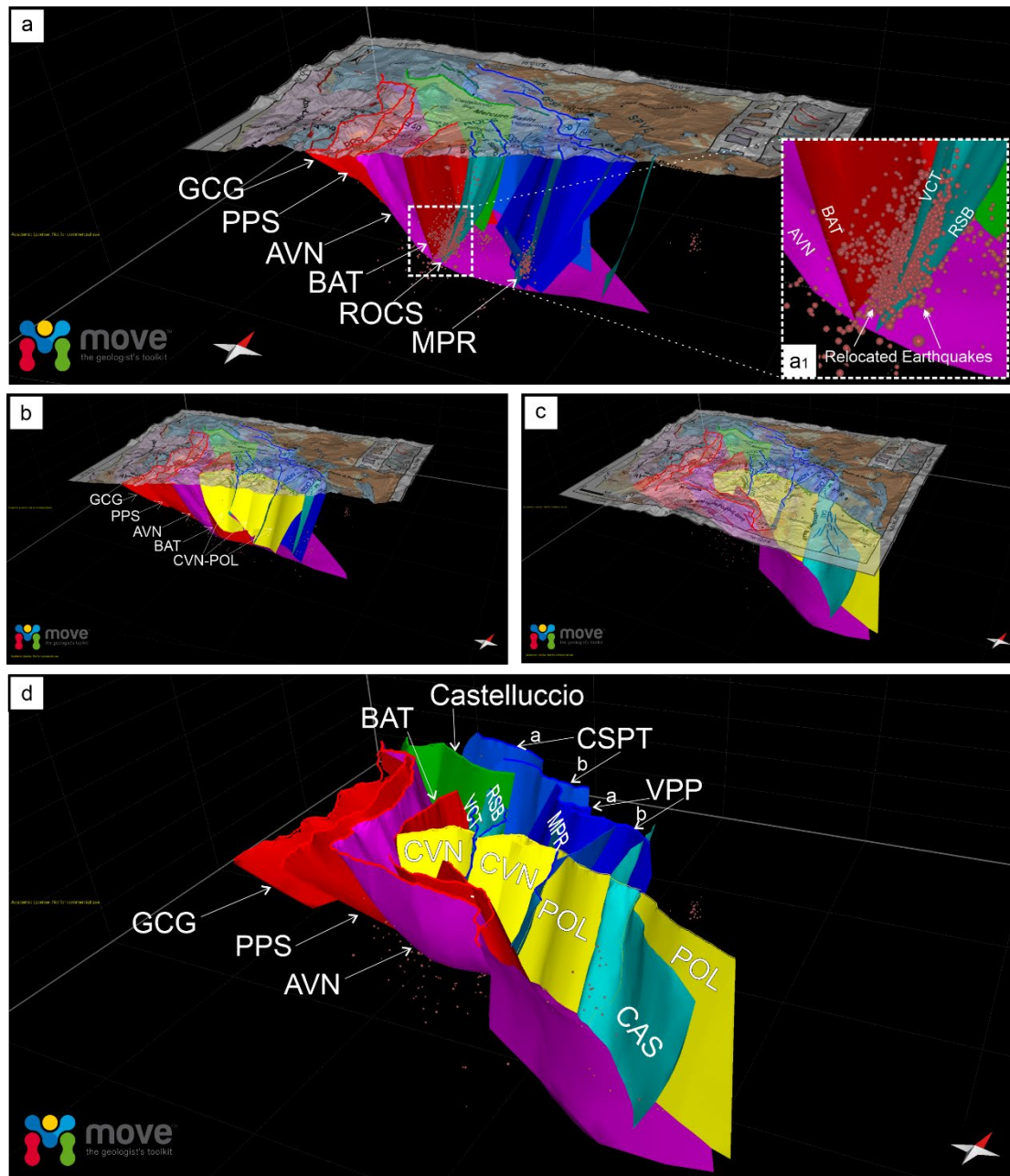


Figure 8: 3D Fault Model of the extensional system at the Calabrian-Lucanian boundary extrapolated down to ~10-12 km. In the panels (a) (b) (c) the geological-structural map (from Brozzetti et al., 2017a) is superimposed over a 10 m-resolution DEM (from Tarquini et al., 2012). The reconstruction of the fault systems is discussed in the paper. In the top panel (a), the lower right inset (a1) shows the detail of the main faults involved during the 2010-2018 seismic activity. (d) 3DFM of all extensional fault realized through the move software. For the acronyms, see supplementary text 1.

425 The faults belonging to the E-NE-dipping CRFS fault set are represented in red and violet, whereas the antithetic ROCS and
426 MPR faults are shown as blue surfaces (fault acronyms as in Fig. 2). The yellow surface is the three-dimensional surface of
427 the POL and its westernmost segment (CVN) bounding, to the north, the Campotenese basin.

428

429

430 **5.4 From 3D Fault Model to expected earthquake magnitude**

431

432 Coherently with what is observed in most Apennine chains (D'Agostino et al., 2001; Ferranti et al., 2014; Montone and
433 Mariucci, 2016; Mariucci and Montone, 2020), the upper crustal Pollino seismicity develops in response to WSW- ENE
434 oriented extension. This is well constrained by the focal solutions of the strongest events (M_w 5.2, 25 October 2012; M_w 4.3,
435 28 May 2012, and M_w 4.0, 6 June 2014 earthquakes) and of all the $M_w \geq 3.5$ earthquakes that occurred during 2010-2014, and
436 with the results of the geological and seismological inversion (Fig. 5). Such consistency suggests that the present stress field
437 is in continuity with the long-term one, which set up at least since the Early-Middle Pleistocene, as already suggested by
438 previous works (Papanikolaou and Roberts, 2007; Brozzetti et al. 2009; 2017a).

439 Comparing the distribution of the whole 2010-2018 seismic activity with the Late Quaternary structures mapped at the surface,
440 we maintain that the ROCS and the MPR faults are suitable as the seismogenic sources for the Mormanno (2012, M_w 5.2) and
441 Morano Calabro (2012, M_w 4.3 and 2014, M_w 4.0) earthquakes, respectively. In addition, our 3DFM allows a parameterization
442 of the sources and their seismogenic potential assessment. The map view of the W-dipping faults (Figs. 9a) depicts irregularly-
443 shaped seismogenic boxes which are delimited to the east by the fault traces (at the surface) and to the west by the branch line
444 of each fault with the base of the seismogenic layer. Some of these boxes include historical or instrumental earthquakes (Fig.
445 9b), while others are not associated with any significant event.

446 The performed 3D reconstruction allowed us to estimate the effective area extent of all the fault segments (Fig. 9c), that, when
447 inserted in the appropriate scaling relationships, provide the expected magnitude possibly releasable in case of entire rupture
448 (Fig. 9c).

449 We also computed the magnitude values obtained using the regressions as a function of the surface fault length (Fig. 9c).
450 Using six different empirical relations (Wells and Coppersmith, 1994; Wesnousky, 2008; Leonard, 2010; Stirling et al., 2013),
451 we compared the values determined for all the investigated active normal faults (Figs. 9d,e).

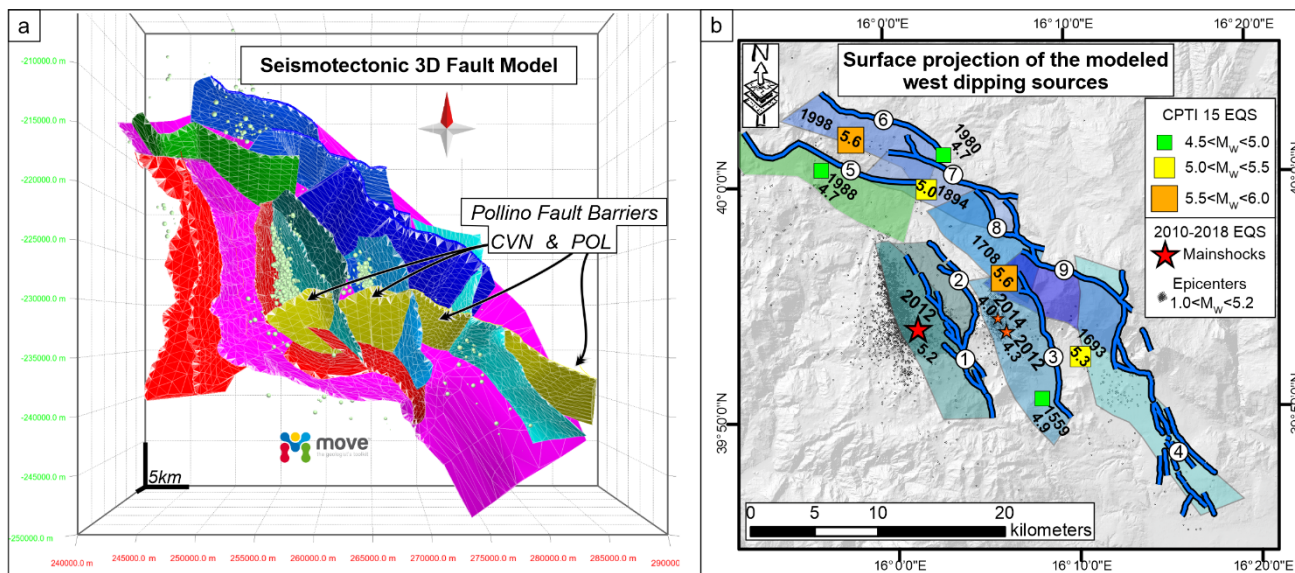
452 It is evident that, for each fault, the expected magnitude computed using fault area is lower than the one calculated by using
453 fault length. The range of variation is narrower for the values calculated on the ground of fault-area regressions (yellow bars
454 in Figs. 9d,e).

455 Given the significant difference in the magnitude values computed using area- or length-based scaling relationships, we
456 suggest that (where possible) the reconstruction of a 3D-fault geometry should be pursued and preferred in order to derive
457 more reliable parameters to be used (Supplementary Table 1). This is even more essential in complex extensional systems as
458 the one we investigated along the Calabrian-Lucanian border.

459 In fact, the 3DFM highlights as the areal extension of the W-dipping faults, depends on their position within the hanging wall
460 of the detachment (see sect. 5.3). This implies that faults with comparable length at the surface may have significantly different
461 areas, depending on the reached depths. The CSPT, VPP and CAS crop out at greatest distance from the GCG break-away
462 zone. Consequently, they intersect the basal detachment at the higher depth and have the maximum area extent among the W-
463 dipping fault set (Fig. 9a,d).

464 By applying the aforementioned scaling laws (Fig. 9) to the W-dipping faults identified to be involved during the 2010-2014
465 seismic activity, we calculated the expected magnitude of $\sim M_w=6.1$ for the VCT and the RSB, and of $\sim M_w=6.2$ for the MPR.
466 Since the two faults (RSB+VCT) of the W-dipping ROCS has been interpreted to join at hypocentral depth to form a single
467 structure (thus a unique seismogenic patch was reconstructed – Fig. 10a), a value of $\sim M_w=6.4$ could be reached in the case of
468 a complete and concurrent ruptures on both the segments. The aforesaid values are sensibly higher than the magnitudes of the
469 earthquakes recorded to date in the Mercure-Campotenese area (Figs. 1b, 9b), thus suggesting that the considered faults may
470 have released only partially their seismogenic potential during historical times.

471 This inference also agrees with the distribution and evolution of the 2010-2018 seismic activity. The clusters of the relocated
472 hypocenters concentrated in the deepest parts of the ROCS and MPR faults (Fig. 6) confirming that only a portion of such
473 faults ruptured during the sequence, without the rupture reaching the surface.



Scaling Relationships for Seismic-Hazard Analysis

Fault Acronym	Area km ²	$M_w(a)$	$M_w(b)$	$M_w(c)$	Length km	$M_w(d)$	$M_w(e)$	$M_w(f)$
VCT (1)	131.07	6.1	6.2	6.1	15.16	6.5	6.7	6.8
RSB (2)	123.39	6.1	6.1	6.1	12.82	6.4	6.7	6.8
ROCS (RSB + VCT)	254.46	6.4	6.4	6.4	27.98	6.8	6.8	7.0
MPR (3)	153.01	6.2	6.2	6.2	13.33	6.4	6.7	6.8
CAS (4)	286.49	6.5	6.5	6.4	20.64	6.6	6.7	6.9
Castelluccio (5)	120.35	6.1	6.1	6.1	16.12	6.5	6.7	6.9
CSPTa (6)	164.35	6.2	6.2	6.2	11.04	6.3	6.6	6.7
CSPTb (7)	171.33	6.2	6.3	6.2	11.28	6.3	6.6	6.7
CSPT a+b	335.68	6.5	6.6	6.5	22.32	6.6	6.8	7.0
VPPa (8)	150.06	6.2	6.2	6.2	8.00	6.1	6.5	6.6
VPPb (9)	129.28	6.1	6.1	6.1	9.49	6.2	6.6	6.7
VPP a+b	279.34	6.5	6.5	6.4	17.50	6.5	6.7	6.9
SVPC (VPP+CSPT)	615.02	6.8	6.8	6.8	39.81	6.9	6.9	7.2

a Leonard 2010 (Area), dip slip

$$M_w = 4.00 + \log A$$

b Wells & Coppersmith 1994 (Area), all slip types

$$M_w = 4.07 + 0.98 \log A$$

c Wells & Copp. 1994 (Area), normal slip

$$M_w = 3.93 + 1.02 \log A$$

d Wells & Copp. 1994 (Length), normal slip

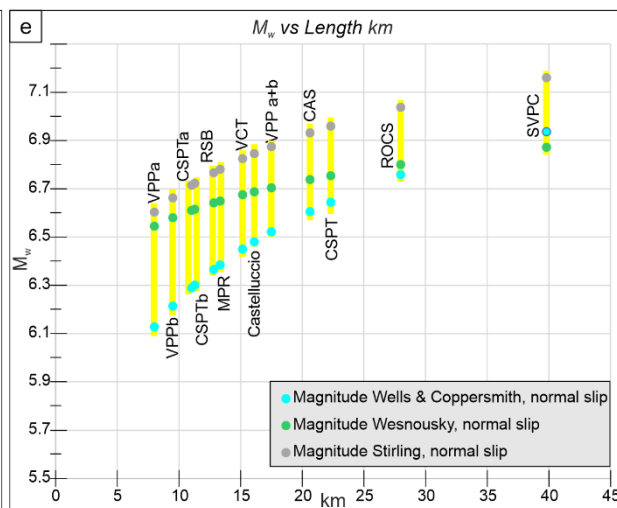
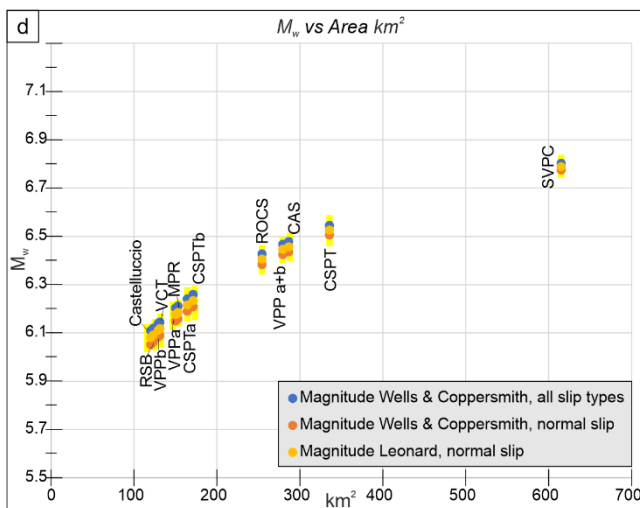
$$M_w = 5.08 + 1.16 \log L$$

e Wesnousky 2008 (Length), normal slip

$$M_w = 6.12 + 0.47 \log L$$

f Stirling et. al. 2013 (Length), normal slip

$$M_w = 5.88 + 0.88 \log L$$



475 **Figure 9:** (a) Seismotectonic 3D Fault Model in map view. (b) Box representation of the W-dipping seismogenic faults
476 belonging to the 3DFM with detailed segmentation pattern. Fault traces are numbered according to the table of the panel (c).
477 The associated historical earthquakes from CPTI15 v3.0 ($4.5 < M_w < 6.0$; Rovida et al., 2020, 2021) and the epicentral
478 distribution of the 2010-2018 seismic activity occurred in the Pollino area ($1.0 < M_w < 5.2$) are also reported. (c) Expected
479 magnitude according to scaling laws (Wells & Coppersmith 1994, Wesnousky 2008, Leonard 2010, Stirling et al. 2013) and
480 calculated based on fault area (A) and length (L).
481 (d-e) comparison of magnitude values calculated for all the investigated active faults, using fault area- (d) and fault length-(e)
482 based scaling relationships.

484 6 Discussion

486 6.1 Seismogenic patches activated during 2010-2014

488 The seismogenic patches activated on the ROCS and MPR faults during the 2010-2014 seismic sequence are considered as the
489 reasonable approximation of the actual portion of the faults which broke during the mainshock and the sequence of the early
490 aftershocks. We obtained them by projecting the relocated hypocenters on the reconstructed fault surface and depicting their
491 distribution using the Kernel density geostatistical analyst, available as a tool of the ESRI ArcGIS software package. The
492 delimitation of each seismogenic patch and its parameterization allowed us to verify the correlation between its dimensions
493 and the magnitude released by each fault during the mainshocks.

494 The temporal analysis of the sequence shows that their overall extent was already well defined within the first 72 hours after
495 the major events. Anyhow, inside the surrounding volumes, some seismicity had started before the mainshock and continued
496 to persist constantly throughout the development of the entire sequence so that they include a percentage \geq of 70% of the whole
497 hypocenter locations. The along-strike elongation and area extent of the patches obtained over the VCT and MPR fault surfaces
498 can be assumed respectively as the effective Subsurface Rupture Length and Rupture Area (RLD and RA in Fig. 10b, and 10c,
499 respectively, according to Wells and Coppersmith, 1994) associated with the M_w 5.2 Mormanno (on VCT fault) and M_w 4.0
500 and 4.3 Morano Calabro (on MPR fault) earthquakes.

501 The parameters obtained for the VCT fault are $RLD = 4.9$ km and $RA = 8.3$ km², while $RLD = 1.2$ km and $RA = 3.6$ km² are
502 assessed for the MPR fault. Introducing the aforesaid parameters in the appropriate scale relationships (Fig. 10b,c), we observe
503 a good agreement between the theoretical magnitudes based on the Subsurface Rupture Length and the magnitudes of the
504 mainshocks. The values obtained for the VCT fault (causative of the M_w 5.2 Mormanno earthquake) are $= M_w$ 5.3, whereas
505 for the MPR fault (causative of the M_w 4.0 and 4.3 Morano Calabro earthquakes) is $M_w = 4.5$. The magnitude calculated using
506 the RA-based relationships provides values slightly lower than expected for the VCT ($4.9 < M_w < 5.0$) and slightly higher for the
507 MPR ($4.5 < M_w < 4.6$). In both cases, however, the magnitude values obtained using the scale relationships differ from those
508 observed by an amount < 0.3 .

509

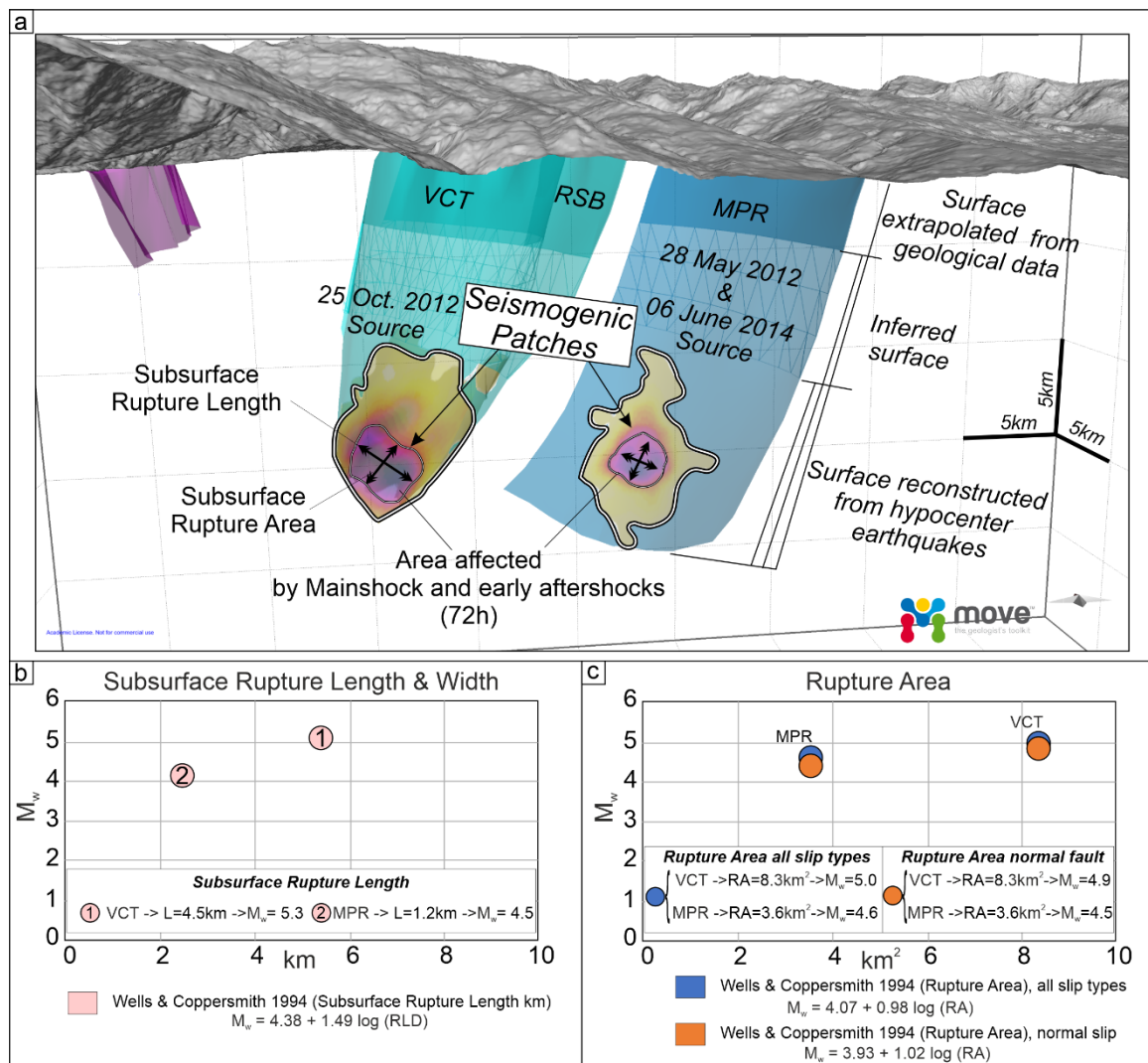


Figure 10: (a) Seismogenic patches activated during the 2010-2014 seismic activity on VCT and MPR faults. Their along-strike elongation and area extent, shown by black arrows, are assumed to be the effective subsurface rupture length and rupture area (RLD and RA, according to Wells and Coppersmith, 1994). The association of the patches' rupture with the M_w 5.2 Mormanno of the 25 October 2012 (on VCT fault) and M_w 4.3 and 4.0 Morano Calabro (on MPR fault, 28 May 2012 and 6 June 2014 respectively) earthquakes is suggested. (b) and (c) show the RLD and RA, respectively, obtained for both the VCT and MPR faults.

6.2 Possible geometric restraints to coseismic rupture propagation

The seismological dataset we used demonstrates that the two main clusters of earthquakes of the 2010-2018 seismicity were generated by as many independent sources related to the sub-parallel, 10 to 15 km-long, ROCS and MPR faults.

523 Brozzetti et al. (2017a) highlighted that the above seismogenic style, characterized by a perpendicular-to-fault strike evolution
524 of the seismic activity, is unlike from those which followed the major instrumental earthquakes recorded in the Apennine
525 Extensional Belt of Italy in recent years, such as the Colfiorito 1997 (M_w 6.0), L'Aquila 2009 (M_w 6.3) and Norcia 2016 (M_w
526 6.5) events (Chiaraluce et al. 2011, 2017; Lavecchia et al., 2011, 2012a, 2016). They also speculated that this peculiar
527 behaviour could have been controlled by the geometric fault pattern of the area, which is characterized by WSW-dipping faults
528 bounded southward by nearly E-W pre-existing structures. These latter are genetically related to the regional-scale, long-lived,
529 “Pollino lineament *s.l.*” (Bousquet, 1969, 1971; Ghisetti and Vezzani, 1982, 1983; Knott and Turco, 1991; Van Dijk et al.,
530 2000) and determine the abrupt contact between the Apennine carbonate platform unit and the San Donato metamorphic core
531 complex (Grandjaquet 1962; Servizio Geologico Nazionale, 1970; Amodio Morelli 1976). The cross-cut relationships detected
532 in the field between the ROCS-MPR set and POL-CVN, highlighted in our 3D model, lead us to exclude the latter fault to
533 have a present seismogenic role, as also supported by the distribution of the instrumental earthquakes which clusterized along
534 with N-S-striking crustal volumes. However, this significant structural-geological boundary, could exert an influence on the
535 southward propagation of the currently active seismogenic faults, driving the eastward transfer of the active extensional
536 deformation belt. This inference is confirmed by the spatial distribution of the hypocentres of the whole 2010-2018 relocated
537 seismicity which is confined within the CVN footwall (Fig. 8d).

538

539 7 Conclusions

540

541 We reconstructed in detail the 3D geometry and kinematics of the interconnected fault pattern responsible for the moderate-
542 magnitude earthquakes which recently affected the Pollino area (Calabrian-Lucanian boundary).

543 The main original outcomes are summarized as follows:

544 - The geological and seismological stress tensors computed using geological- and seismological data demonstrated that they
545 are consistent with a uniform normal faulting regime characterized by an ENE-WSW trending, sub-horizontal σ_3 . This result
546 confirms the coherence between the long-term and the present-day stress field and the persistence of this extensional regime
547 at least since the Middle Pleistocene.

548

549 - The 2010-2018 seismic activity which affected the study area followed a peculiar evolution characterized by the concentration
550 of epicenters in a series of sub-parallel ~NNW-SSE elongated clusters, independent and unconnected, which can be related to
551 two major near-coaxial WSW-dipping faults possibly splaying from a common east-dipping basal detachment and concurrently
552 releasing seismicity.

553

554 - The accurate hypocenter re-locations provided a seismological dataset that was correlated with the active faults mapped at
555 the surface. The hypocenter spatial analysis allows to reconstruct the geometry (3DFM) of the seismogenic sources which
556 released seismicity during 2010-2014 and through 2018. This reconstruction, extrapolated down to the depth of ~10-12 km,

557 was the interpretative key to obtain the overall model of the Quaternary and active extension in the northern Calabria-Lucania
558 Apennines. The 3DFM model includes all the faults playing a significant role, (either direct or indirect), on the seismogenesis
559 of the study area.

560

561 - The western segment of the Pollino Fault (CVN), despite not being currently active, seems to maintain a significant
562 seismotectonic role. In fact, juxtaposing crustal sectors with different structures and compositions (Apennine platform domain
563 to the north, and San Donato metamorphic core to the south) may act as a barrier to the southern propagation of the seismogenic
564 faults of the Mercure-Campotenese sector (ROCS, MPR), limiting their dimensions and seismogenic potential.

565

566 - Based on the dimension and shape of all the active faults of the Pollino area, we estimated the expected magnitudes using
567 appropriate scaling relationships. The complete rupture of individual W-dipping faults which are recognized to have been
568 causative of the 2010-2014 seismic activity, is expected to release a magnitude of $\sim M_w = 6.1$ for the VCT and the RSB, and of
569 $\sim M_w = 6.2$ for the MPR. Higher values, up to $M_w = 6.4$, could be reached in the case of the complete and concurrent rupture on
570 both RSB and VCT. The estimated values exceed the magnitudes of the associate earthquakes which struck the area to date,
571 leading to hypothesize that the aforesaid faults released only partially their seismogenic potential.

572

573 - The delimitation of the fault patches involved during 2010-2014, and their geometrical parameterization, support the
574 consistence between the theoretical magnitudes based on the Subsurface Rupture Length and the magnitudes of the
575 mainshocks.

576 The estimates provided, for the VCT fault (which released the M_w 5.2 Mormanno earthquake) a $M_w = 5.3$, and for the MPR
577 fault (which released the M_w 4.0 and 4.3 Morano Calabro earthquakes) a $M_w = 4.5$. The magnitudes calculated using the
578 relationships based on the Subsurface Rupture Area ($M_w \sim 5.0$ for the VCT and $M_w \sim 4.6$ for the MPR), show slightly greater
579 deviation from the observed values.

580

581 This study pointed out as even in the case of low-to-moderate seismic activity, like the Pollino 2010-2014 one, the approach
582 based on the three-dimensional reconstruction of the Quaternary fault surfaces (both directly involved and neighbouring in the
583 extensional system) represents a real breakthrough in the seismotectonic analysis and, ultimately, in the cognitive path that
584 leads to a better assessment of the seismic hazard of a tectonically active area.

585

586 **Author contribution:** DC, FB conceived and conducted the study. FB, DC, FF, SB wrote the manuscript. DC developed the
587 3D structural-geological model through Move software. DC, SB, FF did GIS analysis and mapping. DC, FB, SB performed
588 the fieldwork. CT, DP, BO, RdN, handled the seismological analysis. FF did the geological and seismological stress-tensor
589 inversion. DC performed the calculation of the expected magnitudes. DC prepared the figures. GL, SB, FB, RdN reviewed the
590 figures. DC, SB prepared the GIS geological database. All authors reviewed the final version of the manuscript.

591

592 **Competing interests:** The authors declare no conflict of interest.

593

594 **Disclaimer.** Publisher’s note: Copernicus Publications remains neutral with regard to jurisdictional claims in published maps
595 and institutional affiliations.

596

597 **Special issue statement.** This article is part of the special issue “Tools, data and models for 3-D seismotectonics: Italy as a key
598 natural laboratory”.

599

600 **Acknowledgements:**

601 The authors are grateful to Petroleum Experts, who provided the Move, 2019.1 suite software license. We are grateful to the
602 Editor Massimiliano Porreca, to Giovanni Barreca and to an anonymous reviewer for improving the manuscript with their
603 review.

604

605 **Financial support.** This research was supported by DPC-INGV PROJECTS-S1 2014-2015 UR-Unich funds, resp. Francesco
606 Brozzetti, and from DiSPUTer Department research funds (resp. Rita de Nardis). This research was also supported by PRIN
607 2017 (2017KT2MKE) funds from the Italian Ministry of Education, University and Research (P.I. Giusy Lavecchia).

608

609 **Review statement.** This paper was edited by Massimiliano Porreca and reviewed by Giovanni Barreca and by an anonymous
610 referee.

611

612 **References**

613

614 Allmendinger, R. W., Cardozo, N., and Fisher, D.: Structural geology algorithms: Vectors and tensors of structural geology:
615 Cambridge, England, Cambridge University Press, 289 pp, <https://doi.org/10.1017/S0016756812000192>, 2012.

616

617 Allmendinger, R.W., Siron, C.R., and Scott, C.P.: Structural data collection with mobile devices: Accuracy, redundancy, and
618 best practices. Journal of Structural Geology, 102, 98-112, <http://dx.doi.org/10.1016/j.jsg.2017.07.011>, 2017.

619

620 Amicucci, L., Barchi, M.R., Montone, P., and Rubilani, N.: The Vallo di Diano and Auletta extensional basins in the southern
621 Apennines (Italy): a simple model for a complex setting, Terra Nova, 20, 475-482, [https://doi.org/10.1111/j.1365-](https://doi.org/10.1111/j.1365-3121.2008.00841.x)
622 [3121.2008.00841.x](https://doi.org/10.1111/j.1365-3121.2008.00841.x), 2008.

623

624 Amodio Morelli, L., Bonardi, G., Colonna, V., Dietrich, D., Giunta, G., Ippolito, F., Liguori, V., Lorenzoni, S., Paglionico,
625 A., Perrone, V., Piccarreta, G., Russo, M., Scandone, P., Zanettin-Lorenzoni, E., and Zuppetta, A.: L'Arco calabro peloritano
626 nell'orogene appenninico-maghrebide, *Mem. Soc. Geol. It.* 17, 1-60, 1976.

627

628 Angelier, J., and Mechler, P. : Sur une méthode graphique de recherche des contraintes principales également utilisable en
629 tectonique et en séismologie: la méthode des dièdres droits, *B. Soc. Géol. Fr.*, 7, 1309–1318, 1977.

630

631 Arrigo, G., Roumelioti, Z., Benetatos, C., Kiratzi, A., Bottari, A., Neri, G., Termini, D., Gorini, A., and Marcucci, S. : A source
632 study of the 9 September 1998 (Mw 5.6) Castelluccio Earthquakes in Southern Italy using Teleseismic and strong motion data,
633 *Nat. Hazards* 37, 245-262, <https://doi.org/10.1007/s11069-005-4644-1>, 2006.

634

635 Ascione, A., Mazzoli, S., Petrosino, P., and Valente, E.: A decoupled kinematic model for active normal faults: insights from
636 the 1980, MS=6.9 Irpinia earthquake, southern Italy, *GSA Bull* 125, 1239-1259, <https://doi.org/10.1130/B30814.1>, 2013.

637

638 Barchi, M. R., De Feyter, A., Magnani, M. B., Minelli, G., Pialli, G., and Sotera, B. M.: Extensional tectonics in the northern
639 Apennines (Italy): Evidence from the CROP03 deep seismic reflection line, *Mem. Soc. Geol. Ital.*, 52, 527– 538, 1998.

640

641 Barchi, M., Lavecchia, G., Galadini, F., Messina, P., Michetti, A. M., Peruzza, L., Pizzi, A., Tondi, E., and Vittori, E.: Sintesi
642 delle conoscenze geologiche sulle faglie responsabili dei terremoti maggiori in Italia Centrale: Parametrizzazione ai fini della
643 caratterizzazione della pericolosità sismica, Gruppo Naz. per la Difesa dai Terremoti, CNR, Rome, 1999.

644

645 Barchi, M., Amato, A., Cippitelli, G., Merlini, S., and Montone, P.: Extensional tectonics and seismicity in the axial zone of
646 the southern Apennines, *Boll. Soc. Geol. It. (Ital. J. Geosci.)* 7, 47-56, 2007.

647

648 Barchi, M.R., Carboni, F., Michele, M., Ercoli, M., Giorgetti, C., Porreca, M., Azzaro, S., and Chiaraluce, L.: The influence
649 of subsurface geology on the distribution of earthquakes during the 2016–2017 Central Italy seismic sequence,
650 *Tectonophysics*, 807, 228797, <https://doi.org/10.1016/j.tecto.2021.228797>, 2021.

651

652 Bello S., de Nardis R., Scarpa R., Brozzetti F., Cirillo D., Ferrarini F., di Lieto B., Arrowsmith R. J., and Lavecchia G.: Fault
653 Pattern and Seismotectonic Style of the Campania-Lucania 1980 Earthquake (Mw 6.9, Southern Italy): New Multidisciplinary
654 Constraints, *Frontiers in Earth Science*, 8, 652, <https://doi.org/10.3389/feart.2020.608063>, 2021a.

655

656 Bello, S., Scott, C. P., Ferrarini, F., Brozzetti, F., Scott, T., Cirillo, D., de Nardis R., Arrowsmith R. J., and Lavecchia G.:
 657 High-resolution surface faulting from the 1983 Idaho Lost River Fault Mw 6.9 earthquake and previous events. *Sci. Data*, 8,
 658 68, 1-20, <https://doi.org/10.1038/s41597-021-00838-6>, 2021b.

659

660 Bello, S., Andrenacci, C., Cirillo, D., Scott, T., Brozzetti, F., Arrowsmith R. J., and Lavecchia G.: High-detail fault
 661 segmentation: Deep insight into the anatomy of the 1983 Borah Peak earthquake rupture zone (Mw 6.9, Idaho, USA),
 662 *Lithosphere*, 8100224, <https://doi.org/10.2113/2021/8100224>, 2021c.

663

664 Blumetti, A. M., Esposito, E., Ferreli, L., Michetti, A. M., Porfido, S., Serva, L., et al.: New data and the reinterpretation of
 665 the November 23, 1980, M 6.9, Irpinia-Lucania earthquake (Southern Apennines) coseismic surface effects, *Spec. Issue Studi*
 666 *Geologici Camerti* 2, 19-27, 2002.

667

668 Bonini, L., Toscani, G., and Seno S. : Three-dimensional segmentation and different rupture behavior during the 2012 Emilia
 669 seismic sequence (Northern Italy), *Tectonophysics*, 630, 33-42, <http://dx.doi.org/10.1016/j.tecto.2014.05.006>, 2014.

670

671 Bousquet, J.C., and Gueremy, P. : Quelques Phénomènes de Néotectonique dans l'Apennin Calabro-Lucanien et Leurs
 672 Conséquences Morphologiques. *Rev. Géogr. Phys. Géol. Dynam* 10, 225-238, 1969.

673

674 Bousquet, J.C.: La tectonique tangentielle des series calcareo-dolomitiques du nord-est de l'Apennin Calabro-Lucanien (Italie
 675 Méridionale). *Geol. Rom.* X, 23-52, 1971.

676

677 Brozzetti, F., and Lavecchia, G.: Seismicity and related extensional stress field: the case of the Norcia Seismic Zone (Central
 678 Italy), *Ann. Tectonicae*, 8(1), 36-57, 1994.

679

680 Brozzetti, F., Lavecchia, G., Mancini, G., Milana G. and Cardinali, M.: Analysis of the 9 September 1998 Mw 5.6 Mercure
 681 earthquake sequence (southern Apennines, Italy): a multidisciplinary approach, *Tectonophysics*, 476, 210-225.
 682 <https://doi.org/10.1016/j.tecto.2008.12.007>, 2009.

683

684 Brozzetti, F.: The Campania-Lucania extensional fault system (southern Italy): a suggestion for a uniform model of active
 685 extension in the Italian Apennines, *Tectonics*, 30 (5), 1-26, TC5009, <http://dx.doi.org/10.1029/2010TC002794>, 2011.

686

687 Brozzetti, F., Cirillo, D., Liberi, F., Faraca, E. and Piluso, E.: The Crati Valley Extensional System: field and subsurface
 688 evidences, *Rend. Online Soc. Geol. It.*, 21, 159-161, 2012.

689

690 Brozzetti, F., Cirillo, D., de Nardis, R., Cardinali, M., Lavecchia, G., Orecchio, B., Presti D., and Totaro, C.: Newly identified
691 active faults in the Pollino seismic gap, southern Italy, and their seismotectonic significance, *J. Struct. Geol.*, 94, 13-31,
692 <https://doi.org/10.1016/j.jsg.2016.10.005>, 2017a.
693

694 Brozzetti, F., Cirillo, D., Liberi, F., Piluso, E., Faraca, E., De Nardis, R., and Lavecchia, G.: Structural style of Quaternary
695 extension in the Crati Valley (Calabrian Arc): Evidence in support of an east-dipping detachment fault, *It. Journ. of Geosci.*,
696 136(3), 434-453, <https://doi.org/10.3301/IJG.2017.11>, 2017b.
697

698 Brozzetti, F., Cirillo, D., and Luchetti, L.: Timing of Contractional Tectonics in the Miocene Foreland Basin System of the
699 Umbria Pre-Apennines (Italy): An Updated Overview, *Geosciences* 2021, 11, 97.
700 <https://doi.org/10.3390/geosciences11020097>, 2021.
701

702 Caiazza, C., Giovine, B., Ortolani, F., Pagliuca, S., Schiattarella, M., Barchi and Vitale, C.: Genesi ed evoluzione strutturale
703 della depressione tettonica dell'alta valle del Fiume Sele (Appennino Campano Lucano), *Stud. Geol. Camerti*, 1992(1), 245–
704 255, 1992.
705

706 Calamita, F., Pizzi, A., and Roscioni, M.: I fasci di faglie recenti ed attive di M. Vettore - M. Bove e di M. Castello - M.
707 Cardosa (Appennino Umbro-Marchigiano), In *Studi Geologici Camerti*; Università di Camerino: Camerino, Italy, 81-95, 1992;
708 Available online: <http://193.204.8.201:8080/jspui/handle/1336/552>, last access: 19 April 2021.
709

710 Castaldo, R., de Nardis, R., De Novellis, V., Ferrarini, F., Lanari, R., Lavecchia, G., et al.: Coseismic stress and strain field
711 changes investigation through 3-D Finite Element modeling of DInSAR and GPS measurements and geological/seismological
712 data: the l'aquila (Italy) 2009 earthquake case study, *J. Geophys. Res. Solid Earth* 123, 4193-4222,
713 <https://doi.org/10.1002/2017JB014453>, 2018.
714

715 Castello, B., Selvaggi, G., Chiarabba, C., and Amato, A.: CSI Catalogo della sismicità italiana 1981-2002, versione 1.1. Roma:
716 INGV-CNT, 2006, <https://csi.rm.ingv.it/>, last access: 19 April 2021.
717

718 Cello, G., Tondi, E., Micarelli, L., and Mattioni L.: Active tectonics and earthquake sources in the epicentral area of the 1857
719 Basilicata earthquake (southern Italy), *Journal of Geodynamics*, 36, 1-2, 37-50, [https://doi.org/10.1016/S0264-3707\(03\)00037-](https://doi.org/10.1016/S0264-3707(03)00037-1)
720 [1](https://doi.org/10.1016/S0264-3707(03)00037-1), 2003.
721

Cheloni, D., D'Agostino, N., Selvaggi, G., Avallone, A., Fornaro, G., Giuliani, R., Reale, D., Sansosti, E., and Tizzani, P.,:
 Aseismic transient during the 2010–2014 seismic swarm: evidence for longer recurrence of $M_I \geq 6.5$ earthquakes in the Pollino
 gap (Southern Italy)?, *Sci. Rep.*, 7(576), <https://doi.org/10.1038/s41598-017-00649-z>, 2017.

Chiaraluce, L., Amato, A., Cocco, M., Chiarabba, C., Selvaggi, G., Di Bona, M., Piccinini, D., Deschamps, A., Margheriti, L.,
 Courboux, F., and Ripepe, M.: Complex normal faulting in the Apennines thrust-and-fold belt: The 1997 seismic sequence
 in Central Italy, *Bull. Seismol. Soc. Am.* 94, 99-116, <https://doi.org/10.1785/0120020052>, 2004.

Chiaraluce, L., Barchi, M.R., Collettini, C., Mirabella, F., and Pucci, S.: Connecting seismically active normal faults with
 Quaternary geological structures: the Colfiorito 1997 case history (Northern Apennines, Italy), *Tectonics* 24, TC1002, 1-16,
<https://doi.org/10.1029/2004TC001627>, 2005.

Chiaraluce, L., Valoroso, L., Piccinini, D., Di Stefano, R., and De Gori, P.: The anatomy of the 2009 L'Aquila normal fault
 system (central Italy) imaged by high resolution foreshock and aftershock locations, *J. Geophys. Res.*, 116, no. B12,
<https://doi.org/10.1029/2011JB008352>, 2011.

Chiaraluce, L., Di Stefano, R., Tinti, E., Scognamiglio, L., Michele, M., Casarotti, E., Cattaneo, M., De Gori, P., Chiarabba,
 C., Monachesi, G., Lombardi, A., Valoroso, L., Latorre, D., and Marzorati, S.: The 2016 Central Italy Seismic Sequence: A
 First Look at the Mainshocks, Aftershocks, and Source Models, *Seismological Research Letters*, 88(3), 757-771,
<https://doi.org/10.1785/0220160221>, 2017.

Cifelli, F., Rossetti, F., and Mattei, M.: The architecture of brittle postorogenic extension: Results from an integrated structural
 and paleomagnetic study in north Calabria (southern Italy), *GSA Bull.*, 119 (1-2), 221-239, <https://doi.org/10.1130/B25900.1>,
 2007.

Cinque, A., Patacca, E., Scandone, P., and Tozzi, M.: Quaternary kinematic evolution of the southern apennines. relationship
 between surface geological features and lithospheric structures, *Ann. Geofisc* 36, 249–260. <https://doi.org/10.4401/ag-4283>,
 1993.

Cinque, A., Ascione, A., and Caiazza, C.: Distribuzione spaziotemporale e caratterizzazione della fagliazione quaternaria in
 Appennino meridionale, in *Le Ricerche del GNDT nel Campo Della Pericolosità Sismica (1996–1999)*, edited by F. Galadini,
 C. Meletti, and A. Rebez, 397 pp., CNR, Gruppo Naz. per la Difesa dai Terremoti, Rome, 2000.

755 Cinti, F. R., Cucci, L., Pantosti, D., D'Addezio, G., and Meghraoui, M.: A major seismogenic fault in a 'silent area': the
 756 Castrovillari fault (Southern Apennines, Italy), *Geophysical Journal International*, 130(3), 595-605, 1997. [https://www.earth-](https://www.earth-prints.org/bitstream/2122/12031/1/text.pdf)
 757 [prints.org/bitstream/2122/12031/1/text.pdf](https://www.earth-prints.org/bitstream/2122/12031/1/text.pdf), last access: 19 April 2021.

758

759 Cinti, F. R., Moro, M., Pantosti, D., Cucci, L., and D'Addezio, G.: New constraints on the seismic history of the Castrovillari
 760 fault in the Pollino gap (Calabria, southern Italy), *J. Seismol.*, 6, 199-217. <https://doi.org/10.1023/A:1015693127008>, 2002.

761

762 Cirillo, D.: Digital Field Mapping and Drone-Aided Survey for Structural Geological Data Collection and Seismic Hazard
 763 Assessment: Case of the 2016 Central Italy Earthquakes, *Applied Sciences*, 10, 5233. <https://doi.org/10.3390/app10155233>,
 764 2020.

765

766 D'Agostino, N., Giuliani, R., Mattone, M., Bonci, L.: Active crustal extension in the central Apennines (Italy) inferred from
 767 GPS measurements in the interval 1994-1999, *Geophysical Research Letters*, 28(10), 2121-2124,
 768 <https://doi.org/10.1029/2000GL012462>, 2001.

769

770 D'Agostino, N.: Complete seismic release of tectonic strain and earthquake recurrence in the Apennines (Italy), *Geophys. Res.*
 771 *Lett* 41, 1155-1162, <https://doi.org/10.1002/2014GL059230>, 2014.

772

773 D'Alessandro, A., Gervasi, A., and Guerra, I.: Evolution and strengthening of the Calabrian regional seismic network. *Adv.*
 774 *Geosciences* 36, 11-16, 2013. <https://adgeo.copernicus.org/articles/36/11/2013/adgeo-36-11-2013.pdf>, last access: 19 April
 775 2021.

776

777 D'Argenio, B.: L'Appennino Campano Lucano. Vecchi e nuovi modelli geologici tra gli anni sessanta e gli inizi degli anni
 778 ottanta. *Mem. Soc. Geol. It.* 41, 3-15, 1992.

779

780 Delaunay, B.: Sur la sphere vide, *Bull. Acad. Sci. USSR(VII)*, Classe Sci. Mat. Nat., 793-800, 1934.

781

782 Delvaux, D., and Sperner, B.: New aspects of tectonic stress inversion with reference to the TENSOR program. In: *New*
 783 *Insights into Structural Interpretation and Modelling* (D.A. Nieuwland, ed.), *J. Geol. Soc. London Spec. Publ.*, 212, 75-100,
 784 2003.

785

786 Delvaux, D., and Barth, A.: African stress pattern from formal inversion of focal mechanism data, *Tectonophysics*, 482, 105-
 787 128, <https://doi.org/10.1016/j.tecto.2009.05.009>, 2010.

788

789 Devoti, R., Esposito, A., Pietrantonio, G., Pisani, A. R., and Riguzzi, F.: Evidence of large-scale deformation patterns from
790 GPS data in the Italian subduction boundary, *Earth Planet. Sci. Lett.* 311 (3-4), 230-241,
791 <https://doi.org/10.1016/j.epsl.2011.09.034>, 2011.

792

793 De Matteis, R., Convertito, V., Napolitano, F., Amoroso, O., Terakawa, T., and Capuano, P.: Pore fluid pressure imaging of
794 the Mt. Pollino region (southern Italy) from earthquake focal mechanisms, *Geophysical Research Letters*, 48,
795 e2021GL094552. <https://doi.org/10.1029/2021GL094552>, 2021.

796

797 Di Bucci, D., Buttinelli, M., D'Ambrogio, C., and Scrocca, D., and the RETRACE-3D Working Group: The RETRACE-3D
798 multi-data and multi-expertise approach towards the construction of a 3D crustal model for the 2016-2018 Central Italy seismic
799 sequence, *Boll. Geof. Teor. Appl.* doi 10.4430/bgta0343, 2021.

800

801 Elter, P., Giglia, G., Tongiorgi, M., and L. Trevisan, L.: Tensional and compressional areas in the recent (Tortonian to present)
802 evolution of the northern Apennines, *Boll. Geofis. Teor. Appl.*, 17, 3-18, 1975.

803

804 Ercoli, M., Pauselli, C., Forte, E., Frigeri, A., and Federico, C.: The Mt. Pollino Fault (southern Apennines, Italy): GPR
805 signature of Holocene earthquakes in a “silent” area. In: *Advanced Ground Penetrating Radar (IWAGPR)*, 2013 7th
806 International Workshop, IEEE, pp. 1-6. <http://dx.doi.org/10.1109/IWAGPR.2013.6601510>, 2013.

807

808 Ercoli, M., Cirillo, D., Pauselli, C., Jol, H. M., and Brozzetti, F.: Ground-penetrating radar signature of Quaternary faulting: a
809 study from the Mt. Pollino region, southern Apennines, Italy, *Solid Earth*, 12, 2573–2596, [https://doi.org/10.5194/se-12-2573-](https://doi.org/10.5194/se-12-2573-2021)
810 [2021](https://doi.org/10.5194/se-12-2573-2021), 2021.

811

812 Faure Walker, J. P., Roberts, G. P., Cowie, P. A., Papanikolaou, I., Michetti, A. M., Sammonds, P., et al.: Relationship between
813 topography, rates of extension and mantle dynamics in the actively-extending Italian Apennines, *Earth Planet Sci. Lett* 325–
814 326, 76–84, <https://doi.org/10.1016/j.epsl.2012.01.028>, 2012.

815

816 Ferranti, L., Palano, M., Cannavò, F., Mazzella, M. E., Oldow, J. S., Gueguen, E., et al.: Rates of geodetic deformation across
817 active faults in southern Italy, *Tectonophysics* 621, 101-122, <https://doi.org/10.1016/j.tecto.2014.02.007>, 2014.

818

819 Ferranti, L., Milano, G., and Pierro, M., Insights on the seismotectonics of the western part of northern Calabria (southern
820 Italy) by integrated geological and geophysical data: coexistence of shallow extensional and deep strike-slip kinematics,
821 *Tectonophysics*, 721, 372-386, <https://doi.org/10.1016/j.tecto.2017.09.020>, 2017.

822

823 Ferrarini, F., Lavecchia, G., de Nardis, R., and Brozzetti, F.: Fault geometry and active stress from earthquakes and field
824 geology data analysis: the Colfiorito 1997 and L'Aquila 2009 cases (central Italy), *Pure Appl. Geoph.*, 172 (5), 1079-1103,
825 <https://doi.org/10.1007/s00024-014-0931-7>, 2015.

826

827 Ferrarini, F., Boncio, P., de Nardis, R., Pappone, G., Cesarano, M., Aucelli, P.P.C., and Lavecchia, G.: Segmentation pattern
828 and structural complexities in seismogenic extensional settings: The North Matese Fault System (Central Italy), *J. Struct.*
829 *Geol.*, 95, 93-112, <http://dx.doi.org/10.1016/j.jsg.2016.11.006>, 2017.

830

831 Ferrarini, F., de Nardis, R., Brozzetti, F., Cirillo, D., Arrowsmith, JR. and Lavecchia, G.: Multiple Lines of Evidence for a
832 Potentially Seismogenic Fault Along the Central-Apennine (Italy) Active Extensional Belt—An Unexpected Outcome of the
833 MW6.5 Norcia 2016 Earthquake, *Front. Earth Sci.*, 9, 642243, <https://doi.org/10.3389/feart.2021.642243>, 2021.

834

835 Filice, F., Liberi, F., Cirillo, D., Pandolfi, L., Marroni, M., and Piluso, E.: Tectonometamorphic and structural evolution of the
836 ophiolitic sequences from the central sector of the Catena Costiera (Northern Calabria), *Rend. Online Soc. Geol. It.*, 21 (1),
837 300-302, 2012.

838

839 Filice, F., Liberi, F., Cirillo, D., Pandolfi, L., Marroni, M., and Piluso, E.: Geological map of the central sector of the Catena
840 Costiera (Northern Calabria), *Rend. Online Soc. Geol. It.*, 29, 55-58, 2013.

841

842 Filice, F., Liberi, F., Cirillo, D., Pandolfi, L., Marroni, M., and Piluso E.: Geology map of the central area of Catena Costiera:
843 insights into the tectono-metamorphic evolution of the Alpine belt in Northern Calabria, *Journal of Maps*, 11(1), 114-125,
844 <https://doi.org/10.1080/17445647.2014.944877>, 2015.

845

846 Filice, F., and Seeber, L.: The Culmination of an Oblique Time-Transgressive Arc Continent Collision: The Pollino Massif
847 Between Calabria and the Southern Apennines, Italy, *Tectonics*, 38(1), 3261-3280. <https://doi.org/10.1029/2017TC004932>,
848 2019.

849

850 Frepoli, A., Cinti, R., Amicucci, L., Cimini, G.B., De Gori, P., and Pierdominici, S.: Pattern of seismicity in the Lucanian
851 Apennines and foredeep (Southern Apennines) from recording by SAPTEX temporary array, *Annal. Geophys.*, 48, 1035-1054,
852 2005. <https://www.earth-prints.org/bitstream/2122/1131/6/manuscript.pdf> , last access: 19 April 2021.

853

854 Frohlich, C.: Display and quantitative assessment of distributions of earthquakes focal mechanisms, *Geophys. J. Int.* 144, 300-
855 308, <https://doi.org/10.1046/j.1365-246x.2001.00341.x>, 2001.

856

857 Gafarov, K., Ercoli, M., Cirillo, D., Pauselli, C., and Brozzetti, F.: Extending surface geology data through GPR prospections:
858 Quaternary faulting signature from the Campotenese area (Calabria-Italy), 17th International Conference on Ground
859 Penetrating Radar, GPR, 8441611, <https://doi.org/10.1109/ICGPR.2018.8441611>, 2018.

860

861 Galadini, F., and Galli, P.: Active tectonics in the Central Apennines (Italy): Input data for seismic hazard assessment, Nat.
862 Hazards, 22, 225-268, <https://doi.org/10.1023/A:1008149531980>, 2000.

863

864 Galli, P., and Peronace, E.: New paleoseismic data from the Irpinia fault. A different seismogenic perspective for the southern
865 Apennines, Earth Sci. Rev. 136, 175-201, <https://doi.org/10.1016/j.earscirev.2014.05.013>, 2014.

866

867 Galli, P.: Recurrence times of central-southern Apennine faults (Italy): Hints from paleoseismology, Terra Nova, 32, 399-407,
868 <https://doi.org/10.1111/ter.12470>, 2020.

869

870 Gephart, J.W., and Forsyth, D.W.: An improved method for determining the regional stress tensor using earthquake focal
871 mechanism data: application to the San Fernando earthquake sequence, J. Geophys. Res., 89, 9305-9320,
872 <https://doi.org/10.1029/JB089iB11p09305>, 1984.

873

874 Ghisetti, F., and Vezzani, L.: Strutture tensionali e compressive indotte da meccanismi profondi lungo la linea del Pollino
875 (Appennino meridionale), Boll. Soc. Geol. It. 101, 385-440, 1982.

876

877 Ghisetti, F., and Vezzani, L.: Structural Map of Mt. Pollino (Southern Italy), 1:50.000 Scale, SELCA, Firenze, 1983.

878

879 Giano, S. I., and Martino, C.: Assetto morfotettonico e morfostratigrafico di alcuni depositi continentali pleistocenici del bacino
880 del Pergola–Melandro (Appennino Lucano), Quaternario 16 (2), 289-297, 2003.

881

882 Gràcia, E., Grevenmeyer, I., Bartolomé, R. et al. : Earthquake crisis unveils the growth of an incipient continental fault system.
883 Nat. Commun. 10, 3482, <https://doi.org/10.1038/s41467-019-11064-5>, 2019.

884

885 Grandjacquet, C.: Données nouvelles sur la tectonique tertiaire des massif Calabro-Lucaniens. Bull. Soc. Geol. Fr. 7ème série
886 4, 695-706, 1962.

887

888 Guerra, I., Harabaglia, P., Gervasi, A., and Rosa, A.B.: The 1998–1999 Pollino (Southern Apennines, Italy) seismic crisis:
889 tomography of a sequence, Ann. Geophys. 48, 995-1007, <https://doi.org/10.4401/ag-3249>, 2005.

890

891 Guidoboni E., Ferrari G., Mariotti D., Comastri A., Tarabusi G., Sgattoni G., and Valensise G.: CFTI5Med, Catalogo dei Forti
892 Terremoti in Italia (461 a.C.-1997) e nell'area Mediterranea (760 a.C.-1500), Istituto Nazionale di Geofisica e Vulcanologia
893 (INGV), <http://storing.ingv.it/cfti/cfti5/>, 2018.

894

895 Guidoboni, E., Ferrari, G., Tarabusi, G., Sgattoni, G., Comastri, A., Mariotti, D., Ciuccarelli, C., Bianchi, M.G., and Valensise
896 G.: CFTI5Med, the new release of the catalogue of strong earthquakes in Italy and in the Mediterranean area, Scientific Data
897 6, article number: 80, <https://doi.org/10.1038/s41597-019-0091-9>, 2019.

898

899 Heidbach, O., Tingay, M., Barth, A., Reinecker, J., Kurfeß, D., and Müller, B.: Global crustal stress pattern based on the world
900 stress map database release 2008, Tectonophysics 482, 3-15, <https://doi.org/10.1016/j.tecto.2009.07.023>, 2010.

901

902 Hippolite, J.C., Angelier, J., and Barrier, E.: Compressional and extensional tectonics in an arc system; example of the Southern
903 Apennines, J. Struct. Geol. 17, 1725–1740, [https://doi.org/10.1016/0191-8141\(95\)00066-M](https://doi.org/10.1016/0191-8141(95)00066-M), 1995.

904

905 Husen, S., and Smith, R.: Probabilistic earthquake location in three-dimensional velocity models for the Yellowstone National
906 Park region, Wyoming, Bull. Seism. Soc. Am. 94 (6), 880-896, 2004.
907 <https://uusatrg.utah.edu/PAPERS/husen2004probeqreloc.pdf>, last access: 19 April 2021.

908

909 Iannace, A., D'Errico, M., and Vitale, S.: Carta Geologica dell'area compresa tra Maratea, Castrovillari e Sanginetto. In: Vitale,
910 S., Iannace, A. (Eds.), Analisi Dello Strain Finito in 3D Dell'Unità Pollino-Ciagola (Confine Calabro-lucano, Italia
911 Meridionale), Studi Geologici Camerti, Nuova Serie, 2, 153-167 (ISSN: 0392-0631), 2004.

912

913 Iannace, A., Garcia Tortosa, F.J., and Vitale, S.: The Triassic metasedimentary successions across the boundary between
914 Southern Apennines and Calabria–Peloritani Arc (Northern Calabria, Italy), Geol. J., 40, 155–171.
915 <https://doi.org/10.1002/gj.1001>, 2005.

916

917 Iannace, A., Vitale, S., D'Errico, M., Mazzoli, S., Di Staso, A., Macaione, E., Messina, A., Reddy, S.M., Somma, R.,
918 Zamparelli, V., Zattin, M., and Bonardi, G.: The carbonate tectonic units of northern Calabria (Italy): a record of Apulian
919 palaeomargin evolution and Miocene convergence, continental crust subduction, and exhumation of HP–LT rocks, J. Geol.
920 Soc. Lond. 164, 1165-1186. <https://doi.org/10.1144/0016-76492007-017>, 2007.

921

922 Ietto, A., and Barilaro, A.M.: L'Unità di San Donato quale margine deformato Cretacico-Paleogene del bacino di Lagonegro
923 (Appennino Meridionale-Arco Calabro), Boll. Soc. Geol. It. 112, 477-496, 1993.

924

925 ISIDe Working Group: Italian Seismological Instrumental and Parametric Database (ISIDe). Istituto Nazionale di Geofisica e
 926 Vulcanologia (INGV), <https://doi.org/10.13127/ISIDE>, last access: 19 April 2021, 2007.

927

928 Johnson, K., Nissen, E., Saripalli, S., Arrowsmith, J.R., McGarey, P., Scharer, K., Williams, P., Blisniuk, K.: Rapid mapping
 929 of ultrafine fault zone topography with structure from motion, *Geosphere*, 10, 969-986, <https://doi.org/10.1130/GES01017.1>,
 930 2014.

931

932 Klin, P., Laurenzano, G., Romano, M.A., Priolo, E., Martelli, L.: ER3D: a structural and geophysical 3-D model of central
 933 Emilia-Romagna (northern Italy) for numerical simulation of earthquake ground motion, *Solid Earth*, 743, 10:931–949.
 934 <https://doi.org/10.5194/se-10-931-2019>, 2019.

935

936 Knott, S.D., and Turco, E.: Late cenozoic kinematics of the Calabrian arc, southern Italy. *Tectonics* 10 (6), 1164-1172, 1991.

937

938 Lavecchia, G., Brozzetti, F., Barchi, M., Menichetti, M., and Keller, J. V. A.: Seismotectonic zoning in east-central Italy
 939 deduced from an analysis of the Neogene to present deformations and related stress fields, *Geol. Soc. Am. Bull.* 106, 1170-
 940 1120, doi:10.1130/0016, [https://doi.org/10.1130/0016-7606\(1994\)106%3C1107:SZIECI%3E2.3.CO;2](https://doi.org/10.1130/0016-7606(1994)106%3C1107:SZIECI%3E2.3.CO;2), 1994.

941

942 Lavecchia, G., Boncio, P., Brozzetti, F., De Nardis, R., Di Naccio, D., Ferrarini, F., Pizzi, A., and Pomposo, G.: The April
 943 2009 L'Aquila (central Italy) seismic sequence (Mw 6.3): a preliminary seismotectonic picture, *Recent Prog. Earthquake Geol.*
 944 2011, 1-17, ISBN: 978-1-60876-147-0, 2011.

945

946 Lavecchia, G., Ferrarini, F., Brozzetti, F., de Nardis, R., Boncio, P., and Chiaraluce, L.: From surface geology to aftershock
 947 analysis: constraints on the geometry of the L'Aquila 2009 seismogenic fault system, *Italian J. Geosciences* 131 (3), 330-347,
 948 <https://doi.org/10.3301/IJG.2012.24>, 2012a.

949

950 Lavecchia, G., de Nardis, R., Cirillo, D., Brozzetti, F., and Boncio, P.: The May-June 2012 Ferrara Arc earthquakes (northern
 951 Italy): structural control of the spatial evolution of the seismic sequence and of the surface pattern of coseismic fractures,
 952 *Annals of Geophysics*, 55, 4, <https://doi.org/10.4401/ag-6173>, 2012b.

953

954 Lavecchia G., de Nardis, R., Costa, G., Tiberi, L., Ferrarini, F., Cirillo, D., Brozzetti F., and Suhadolc, P.: Was the Mirandola
 955 thrust really involved in the Emilia 2012 seismic sequence (northern Italy)? Implications on the likelihood of triggered
 956 seismicity effects, *Boll. Geof. Teor. Appl.*, Vol. 56 (4), 461-488, http://www3.inogs.it/bgo/provavpage.php?id_articolo=673 ,
 957 last access: 19 April 2021, 2015.

958

959 Lavecchia, G., Castaldo, R., de Nardis, R., De Novellis, V., Ferrarini, F., Pepe, S., Brozzetti, F., Solaro, G., Cirillo, D., Bonano,
 960 M., Boncio, P., Casi, F., De Luca, C., Lanar, R., Manunta, M., Manzo, M., Pepe, A., Zinno, I., and Tizzani, P.: Ground
 961 deformation and source geometry of the 24 August 2016 Amatrice earthquake (Central Italy) investigated through analytical
 962 and numerical modeling of DInSAR measurements and structural-geological data, *Geophys. Res. Lett.*, 43,
 963 <https://doi.org/10.1002/2016GL071723>, 2016
 964
 965 Lavecchia, G., Adinolfi, G. M., de Nardis, R., Ferrarini, F., Cirillo, D., Brozzetti, F., De Matteis, R., Festa, G., and Zollo, A.:
 966 Multidisciplinary inferences on a newly recognized active east-dipping extensional system in central Italy, *Terra Nova*, 29,
 967 77–89, <https://doi.org/10.1111/ter.12251>, 2017.
 968
 969 Lavecchia, G., de Nardis, R., Ferrarini, F., Cirillo, D., Bello, S., and Brozzetti, F.: Regional seismotectonic zonation of
 970 hydrocarbon fields in active thrust belts: a case study from Italy, in *Building knowledge for geohazard assessment and*
 971 *management in the caucasus and other orogenic regions*, Editors F. L. Bonali, F. Pasquaré Mariotto, and N. Tsereteli (the
 972 Netherlands: Springer), https://doi.org/10.1007/978-94-024-2046-3_7, 2021.
 973
 974 Leonard, M.: Earthquake fault scaling: Relating rupture length, width, average displacement, and moment release, *Bull.*
 975 *Seismol. Soc. Am.*, 100(5A), 1971–1988. <https://doi.org/10.1785/0120090189>, 2010.
 976
 977 Liberi, F., Morten, L., and Piluso, E.: Geodynamic significance of the ophiolites within the Calabrian Arc, *Island Arc*, 15, 26–
 978 43, <https://doi.org/10.1111/j.1440-1738.2006.00520.x>, 2006.
 979
 980 Liberi, F., and Piluso, E.: Tectonometamorphic evolution of the ophiolitic sequences from Northern Calabrian Arc, *Italian*
 981 *Journal Geoscience (Boll. Society Geological Italian)*, 128, 483–493, <https://doi.org/10.3301/IJG.2009.128.2.483>, 2009.
 982
 983 Lippmann-Provansal, M. : L'Appennin meridionale (Italie): Etude geomorphologique, these Doctorat, Univ. D'Aix-Marseille
 984 II, Marseille, France, 1987.
 985
 986 Lomax, A., Virieux, J., Volant, P., and Berge-Thierry, C.: Probabilistic Earthquake Location in 3D and Layered Model, in
 987 *Advances in Seismic Event Location*, Pp. 101–134, Kluwer Academic Publishers, Netherlands, 2000.
 988
 989 Margheriti, L., Amato, A., Braun, T., Cecere, G., D'Ambrosio, C., De Gori, and P., Selvaggi, G.: Emergenza nell'area del
 990 Pollino: le attività della Rete Sismica Mobile, *Rapporti Tecnici INGV*, 2013.
 991

992 Mariucci, M.T., and Montone, P.: Database of Italian present-day stress indicators, IPSI 1.4, Sci. Data 7, 298.
 993 <https://doi.org/10.1038/s41597-020-00640-w>, 2020.
 994
 995 Maschio, L., Ferranti, L., and Burrato, P.: Active extension in Val d'Agri area, southern Apennines, Italy: Implications for the
 996 geometry of the seismogenic belt, Geophys. J. Int., 162, 591-609, <https://doi.org/10.1111/j.1365-246X.2005.02597.x>, 2005.
 997
 998 Mattei, M., Cifelli, F., and D'Agostino N.: The evolution of the Calabrian Arc: Evidence from paleomagnetic and GPS
 999 observations, Earth and Planetary Science Letters, 263 (3-4), 259-274, <https://doi.org/10.1016/j.epsl.2007.08.034>, 2007.
 1000
 1001 Michetti, A. M., Ferreli, L., Serva, L., and Vittori, E.: Geological evidence for strong historical earthquakes in an "aseismic"
 1002 region: The Pollino case (Southern Italy), Journal of Geodynamics, 24:1-4, 67-86. [https://doi.org/10.1016/S0264-](https://doi.org/10.1016/S0264-3707(97)00018-5)
 1003 [3707\(97\)00018-5](https://doi.org/10.1016/S0264-3707(97)00018-5), 1997.
 1004
 1005 Michetti, A. M., Ferreli, L., Esposito, E., Porfido, S., Blumetti, A. M., Vittori, E., Serva, L., and Roberts, G. P.: Ground Effects
 1006 during the 9 September 1998, Mw = 5.6 Lauria, Earthquake and the Seismic Potential of the seismic Pollino Region in Southern
 1007 Italy, Seismological Research Letters, 71(1), 31-46. <https://doi.org/10.1785/gssrl.71.1.31>, 2000.
 1008
 1009 Montone, P., and Mariucci, M.T.: The New Release of the Italian Contemporary Stress Map, Geophys. J. Int., 205 (3), 1525–
 1010 1531. <https://doi.org/10.1093/gji/ggw100>, 2016.
 1011
 1012 Mostardini, F., and Merlini, S.: Appennino centro meridionale - Sezioni geologiche e proposta di modello strutturale. Mem.
 1013 Soc. Geol. Ital. 35, 177–202, 1986
 1014
 1015 Napolitano, F., De Siena, L., Gervasi, A., Guerra, I., Scarpa, R., and La Rocca, M.: Scattering and absorption imaging of a
 1016 highly fractured fluid-filled seismogenic volume in a region of slow deformation, Geosci. Front., 11(3), 989-998.
 1017 <https://doi.org/10.1016/j.gsf.2019.09.014>, 2020.
 1018
 1019 Napolitano, F., Galluzzo, D., Gervasi, A., Scarpa, R., La Rocca, M.: Fault imaging at Mt Pollino (Italy) from relative location
 1020 of microearthquakes, Geophysical Journal International, 224(1), 637-648, <https://doi.org/10.1093/gji/ggaa407>, 2021.
 1021
 1022 Nicholson, G., Plesch, A., Sorlion, C. C., Shaw, J. H., and Hauksson, E.: TheSCEC 3D community fault model (CFM-v5): an
 1023 updated and expanded fault set of oblique crustal deformation and complex fault interaction for southern California, Eos Trans.
 1024 Am. Geophys. Union 95 (52). Abstract T31B-4584, 2014.
 1025

1026 Nicholson, C., Plesch, A., Sorlien, C. C., Shaw, J. H., and Hauksson, E.: The SCEC community fault model version 5.0: an
 1027 updated and expanded 3D fault set for southern California, in 2015 pacific section AAPG joint meeting program (Oxnard,
 1028 CA), Vol. 77, September 12-16, 2015.
 1029
 1030 Novakova, L., and Pavlis, T.L.: Assessment of the precision of smart phones and tablets for measurement of planar
 1031 orientations: A case study, *Journal of Structural Geology*, 97, <https://doi.org/10.1016/j.jsg.2017.02.015>, 2017.
 1032
 1033 Ogniben, L.: Schema introduttivo alla geologia del confine calabro-lucano, *Mem. Soc. Geol. It*, 8, 453-763, 1969.
 1034
 1035 Ogniben, L.: Schema geologico della Calabria in base ai dati odierni, *Geologia Romana*, 12, 243-585, 1973.
 1036
 1037 Orecchio, B., Presti, D., Totaro, C., Guerra, I., and Neri, G.: Imaging the velocity structure of the Calabrian Arc region (south
 1038 Italy) through the integration of different seismological data, *Boll. Geofis. Teor. Appl.* 52, 625-638, 2011,
 1039 http://www3.ogs.trieste.it/bgta/pdf/bgta0023_ORECCHIO.pdf last access: 19 April 2021.
 1040
 1041 Pantosti, D., and Valensise, G.: Faulting mechanism and complexity of the november 23, 1980, Campania-Lucania earthquake,
 1042 inferred from surface observation, *J. Geophys. Res.*, 95, 15319-15341, <https://doi.org/10.1029/JB095iB10p15319>, 1990.
 1043
 1044 Pantosti, D., and Valensise, G.: Source geometry and long-term behavior of the 1980, Irpinia earthquake fault based on field
 1045 geologic observations. *Ann. Geofisc* 36, 41–49. <https://doi.org/10.4401/ag-4299>, 1993.
 1046
 1047 Papanikolaou, I. D., and Roberts, G. P.: Geometry, kinematics and deformation rates along the active normal fault system in
 1048 the southern Apennines: implications for fault growth, *J. Struct. Geol* 29, 166-188. <https://doi.org/10.1016/j.jsg.2006.07.009>,
 1049 2007.
 1050
 1051 Passarelli, L., Hainzl, S., Cesca, S., Meccaferri, F., Mucciarelli, M., Roessler, D., Corbi, F., Dahm, T., and Rivalta, E.: Aseismic
 1052 transient driving the swarm-like seismic sequence in the Pollino range, Southern Italy, *Geophys. J. Int.*, 201(3), 1553-1567,
 1053 <https://doi.org/10.1093/gji/ggv111>, 2015.
 1054
 1055 Pastori, M., Margheriti, L., De Gori, P., Govoni, A., Lucente, F.P., Moretti, M., Marchetti, A., Di Giovambattista, R., Anselmi,
 1056 M., De Luca, P., Nardi, A., Agostinetti, N.P., Latorre, D., Piccinini, D., Passarelli, L., and Chiarabba, C.: The 2011–2014
 1057 Pollino Seismic Swarm: Complex Fault Systems, Imaged by 1D Refined Location and Shear Wave Splitting Analysis at the
 1058 Apennines–Calabrian Arc Boundary, *Front. Earth Sci.*, 9, 618293, <https://doi.org/10.3389/feart.2021.618293>, 2021.
 1059

1060 Patacca, E., and Scandone, P.: Geological interpretation of the CROP-04 seismic line (Southern Apennines, Italy), *Boll. Soc.*
 1061 *Geol. It. (Ital. J. Geosci.)*, 7, 297-315, 2007.
 1062
 1063 Petroleum Experts (PetEx Ltd.) MOVE structural geology software, [https://www.petex.com/products/move-suite/digital-field-](https://www.petex.com/products/move-suite/digital-field-mapping/)
 1064 [mapping/](https://www.petex.com/products/move-suite/digital-field-mapping/), last access: 19 April 2021.
 1065
 1066 Plesch, A., Shaw, J. H., and Jordan, T. H.: Stochastic descriptions of basin velocity structure from analyses of sonic logs and
 1067 the SCEC community velocity model (CVM-H), in Presentation at 2014 SSA annual meeting, Palm Springs, CA, September
 1068 6-10, 2014.
 1069
 1070 Pondrelli, S., Salimbeni, S., Ekström, G., and Morelli, A.: The Italian CMT dataset from 1977 to the present, *Phys. Earth*
 1071 *Planet*, In 159, 286–303, <https://doi.org/10.1016/j.pepi.2006.07.008>, 2006.
 1072
 1073 Porreca, M., Minelli, G., Ercoli, M., Brobia, A., Mancinelli, P., Cruciani, F., Giorgetti, C., Carboni, F., Mirabella, F., Cavinato,
 1074 G., Cannata, A., Pauselli, C., and Barchi, M. R.: Seismic reflection profiles and subsurface geology of the area interested by
 1075 the 2016–2017 earthquake sequence (Central Italy), in: The 2016 Central Italy Seismic Sequence: Insights, implications and
 1076 lessons learned, *Tectonics*, 37, 1116–1137, <https://doi.org/10.1002/2017TC004915>, 2018.
 1077
 1078 Porreca, M., Fabbrizzi, A., Azzaro, S., Pucci, S., Del Rio, L., Pierantoni, P. P., Giorgetti, C., Roberts, G., and Barchi, M. R.:
 1079 3D geological reconstruction of the M. Vettore seismogenic fault system (Central Apennines, Italy): Cross-cutting relationship
 1080 with the M. Sibillini thrust, *J. Struct. Geol.*, 131, 103938, <https://doi.org/10.1016/j.jsg.2019.103938>, 2020.
 1081
 1082 Presti, D., Troise, C., and De Natale, G.: Probabilistic location of seismic sequences in heterogeneous media, *Bull. Seismol.*
 1083 *Soc. Am.* 94, 2239-2253, doi: 10.1785/0120030160, 2004.
 1084
 1085 Presti, D., Orecchio, B., Falcone, G., and Neri, G.: Linear versus nonlinear earthquake location and seismogenic fault detection
 1086 in the southern Tyrrhenian Sea. Italy, *Geophys. J. Int.* 172, 607-618, <https://doi.org/10.1111/j.1365-246X.2007.03642.x>, 2008.
 1087
 1088 Robustelli, G., Russo Ermolli, E., Petrosino, P., Jicha, B., Sardella, R., and Donato, P.: Tectonic and climatic control on
 1089 geomorphological and sedimentary evolution of the Mercure basin, southern Apennines, Italy, *Geomorphology* 214, 423-435,
 1090 <https://doi.org/10.1016/j.geomorph.2014.02.026>, 2014.
 1091
 1092 Ross, Z. E., Cochran, E. S., Trugman, D. T., and Smith, J.D.: 3D Fault Architecture Controls the Dynamism of Earthquake
 1093 Swarms, *Science* 368, 1357-1361, <https://doi.org/10.1016/j.jsg.2019.103934>, 2020.

1094

1095 Rovida, A., Locati, M., Camassi, R., Lolli, B., and Gasperini, P.: The Italian earthquake catalogue CPTI15, Bulletin of
1096 Earthquake Engineering, 18, 2953-2984, <https://doi.org/10.1007/s10518-020-00818-y>, 2020.

1097

1098 Rovida A., Locati M., Camassi R., Lolli B., Gasperini P., and Antonucci A.: Catalogo Parametrico dei Terremoti Italiani
1099 (CPTI15), versione 3.0. Istituto Nazionale di Geofisica e Vulcanologia (INGV). <https://doi.org/10.13127/CPTI/CPTI15.3>,
1100 2021.

1101

1102 Sato, H., Hirata, H., Ito, T., Tsumura, N., and Ikawa, T.: Seismic reflection profiling across the seismogenic fault of the 1995
1103 Kobe earthquake, southwestern Japan, Tectonophysics, 286 (1–4), 19-30, [https://doi.org/10.1016/S0040-1951\(97\)00252-7](https://doi.org/10.1016/S0040-1951(97)00252-7),
1104 1998.

1105

1106 SCEC, 2021 <https://www.scec.org/research/cfm>; last access: 19 April 2021.

1107

1108 Schiattarella, M., Torrente, M., and Russo, F.: Analisi strutturale ed osservazioni morfotettoniche nel bacino del Mercure
1109 (Confine calabro-lucano), Il Quaternario, 7, 613-626, 1994.

1110

1111 Scognamiglio, L., Tinti, E., and Quintiliani, M.: Time Domain Moment Tensor (TDMT) [Data set]. Istituto Nazionale di
1112 Geofisica e Vulcanologia (INGV). <https://doi.org/10.13127/TDMT>, 2006.

1113

1114 Servizio Geologico d'Italia: 220 Verbicaro sheet of the Carta Geologica D'Italia, 1: 100.000 Scale. Rome, 1970.

1115

1116 Sgambato, C., Walker, J. P. F., and Roberts, G. P.: Uncertainty in strain-rate from field measurements of the geometry, rates
1117 and kinematics of active normal faults: implications for seismic hazard assessment, J. Struct. Geol. 131, 103934,
1118 <https://doi.org/10.1016/j.jsg.2019.103934>, 2020.

1119

1120 Sketsiou, P., De Siena, L., Gabrielli, S., and Napolitano, F.: 3-D attenuation image of fluid storage and tectonic interactions
1121 across the Pollino fault network, Geophysical Journal International, 226(1), 536–547, <https://doi.org/10.1093/gji/ggab109>,
1122 2021.

1123

1124 Sperner, B., Müller, B., Heidbach, O., Delvaux, D., Reinecker, J., and Fuchs, K.: Tectonic stress in the Earth's crust: advances
1125 in the World Stress Map project. In: New Insights into Structural Interpretation and Modelling (D.A. Nieuwland, ed.), J. Geol.
1126 Soc. London Spec. Publ., 212, 101–116, <https://doi.org/10.1144/GSL.SP.2003.212.01.07>, 2003.

1127

1128 Spina, V., Galli, P., Tondi, E., and Mazzoli, S.: Fault propagation in a seismic gap area (northern Calabria, Italy): implications
 1129 for seismic hazard, *Tectonophysics*, 476, 357-369, <https://doi.org/10.1016/j.tecto.2009.02.001>, 2009.

1130

1131 Stirling, M., Goded, T., Berryman, K. and Litchfield, N.: Selection of Earthquake Scaling Relationships for Seismic-Hazard
 1132 Analysis, *Bulletin of the Seismological Society of America*, 103(6), 2993-3011. <https://doi.org/10.1785/0120130052>, 2013.

1133

1134 Tangari, A.C., Scarciglia, F., Piluso, E., Marinangeli, L., and Pompilio, L.: Role of weathering of pillow basalt, pyroclastic
 1135 input and geomorphic processes on the genesis of the Monte Cerviero upland soils (Calabria, Italy), *Catena*, 171, 299-315,
 1136 ISSN 0341-8162, <https://doi.org/10.1016/j.catena.2018.07.015>, 2018.

1137

1138 Tarquini, S., Vinci, S., Favalli, M., Doumaz, F., Fornaciai, A., and Nannipieri, L.: Release of a 10-m-resolution DEM for the
 1139 Italian territory: Comparison with global-coverage DEMs and anaglyph-mode exploration via the web, *Computers and*
 1140 *Geosciences*, 38, 168-170. <https://doi.org/10.1016/j.cageo.2011.04.018>, 2012.

1141

1142 TDMT database – INGV <http://cnt.rm.ingv.it/tdmt>. last access: 19 April 2021.

1143

1144 Tertulliani, A., and Cucci, L.: New insights on the strongest historical earthquake in the Pollino region (southern Italy),
 1145 *Seismol. Res. Lett.*, 85(3), 743-751, <https://doi.org/10.1785/0220130217>, 2014.

1146

1147 Testa, A., Boncio, P., Di Donato, M., Mataloni, G., Brozzetti, F., and Cirillo, D.: Mapping the geology of the 2016 Central
 1148 Italy earthquake fault (Mt. Vettore – Mt. Bove fault, Sibillini Mts.): geological details on the Cupi – Ussita and Mt. Bove –
 1149 Mt. Porche segments and overall pattern of coseismic surface faulting, *Geological Field Trips and Maps, Italian Geological*
 1150 *Society and of the Geological Survey of Italy*, 11, 1–13, <https://doi.org/10.3301/GFT.2019.03>, 2019.

1151

1152 Totaro, C., Presti, D., Billi, A., Gervasi, A., Orecchio, B., Guerra, I., and Neri, G.: The ongoing seismic sequence at the Pollino
 1153 Mountains, Italy. *Seismol. Res. Lett.*, 84(6), 955-962, <https://doi.org/10.1785/0220120194>, 2013.

1154

1155 Totaro, C., Koulakov, I., Orecchio, B., and Presti, D.: Detailed crustal structure in the area of the southern Apennines–Calabrian
 1156 Arc border from local earthquake tomography, *J. Geodyn.*, 82, 87-97, <https://doi.org/10.1016/j.jog.2014.07.004>, 2014.

1157

1158 Totaro, C., Seeber, L., Waldhauser, F., Steckler, M., Gervasi, A., Guerra, I., Orecchio, B., and Presti, D.: An intense earthquake
 1159 swarm in the southernmost Apennines: fault architecture from high-resolution hypocenters and focal mechanisms, *Bull.*
 1160 *Seismol. Soc. Am.* 105, 1-6. <https://doi.org/10.1785/0120150074>, 2015.

1161

1162 Totaro, C., Orecchio, B., Presti, D., Scolaro, S., and Neri G.: Seismogenic stress field estimation in the Calabrian Arc region
 1163 (south Italy) from a Bayesian approach, *Geophys. Res. Lett.*, 43, 8960–8969, <https://doi.org/10.1002/2016GL070107>, 2016.
 1164
 1165 Valoroso, L., Chiaraluce, L., Di Stefano, R., and Monachesi, G.: Mixed-Mode Slip Behavior of the Altotiberina Low-Angle
 1166 Normal Fault System (Northern Apennines, Italy) through High-Resolution Earthquake Locations and Repeating Events, *J.*
 1167 *Geoph. Res. Solid Earth*, 122(12), 10220-10240, <https://doi.org/10.1002/2017JB014607>, 2017.
 1168
 1169 Van Dijk, J.P., Bello, M., Brancaleoni, G.P., Cantarella, G., Costa, V., Frixia, A., Golfetto, F., Merlini, S., Riva, M., Toricelli,
 1170 S., Toscano, C., and Zerilli, A.: A regional structural model for the northern sector of the Calabrian Arc (southern Italy),
 1171 *Tectonophysics* 324, 267-320, [https://doi.org/10.1016/S0040-1951\(00\)00139-6](https://doi.org/10.1016/S0040-1951(00)00139-6), 2000.
 1172
 1173 Vezzani, L., Festa, A., and Ghisetti, F.C.: Geology and tectonic evolution of the Central-Southern Apennines, Italy, *Special*
 1174 *Paper of the Geological Society of America*, 469, 1-58, <https://doi.org/10.1130/SPE469>, 2010.
 1175
 1176 Villani, F., and Pierdominici, S.: Late Quaternary tectonics of the Vallo di Diano basin (southern Apennines, Italy), *Quat. Sci.*
 1177 *Rev.*, 29, 3167-3183. <https://doi.org/10.1016/j.quascirev.2010.07.003>, 2010
 1178
 1179 Waldhauser F., and Ellsworth W.: A Double-Difference Earthquake Location Algorithm: Method and Application to the
 1180 Northern Hayward Fault, California, *Bull. Seism. Soc. Am.* 90(6):1353-1368, <http://dx.doi.org/10.1785/0120000006>, 2000.
 1181
 1182 Waldhauser, F.: HypoDD: a Computer Program to Compute Double Difference Earthquake Locations. U.S. Geol. Surv, Menlo
 1183 Park, California, pp. 01-113. Open-File Report, 2001.
 1184
 1185 Wells, D.L., and Coppersmith, K.J.: New empirical relationships among magnitude, rupture length, rupture width, rupture
 1186 area, and surface displacement, *Bull. Seismol. Soc. Am.*, 84(4), 974-1002, 1994.
 1187
 1188 Wesnousky, S.G.: Displacement and geometrical characteristics of earthquake surface ruptures: Issues and implications for
 1189 seismic hazard analysis and the process of earthquake rupture, *Bull. Seismol. Soc. Am.*, 98(4), 1609-1632.
 1190 <https://doi.org/10.1785/0120070111>, 2008.
 1191
 1192 Westoby, M.J., Brasington, J., Glasser, N.F., Hambrey, M.J., and Reynolds, J.M.: ‘Structure-from-motion’ photogrammetry:
 1193 A low-cost, effective tool for geoscience applications, *Geomorphology*, 179, 300-314,
 1194 <https://doi.org/10.1016/j.geomorph.2012.08.021>, 2012.